CR-114413

(NASA-CR-114413) AMES HEAT PIPE EXPERIMENT (AHPE) EXPERIMENT DESCRIPTION DOCUMENT (TRW Systems Group) 133 p CSCL 13K

N75-23880

Unclas

00/34 23044

AMES HEAT PIPE EXPERIMENT (AHPE) EXPERIMENT DESCRIPTION DOCUMENT

JANUARY 1972

TRW DOCUMENT NO. 13111-6033-R0-00

PREPARED BY

B. D. MARCUS

CONTRACT NO. NAS 2-5503

PREPARED FOR

NASA—AMES RESEARCH CENTER
MOFFET FIELD, CALIFORNIA 93405

MATERIALS SCIENCE STAFF

TRW
SYSTEMS GROUP

CR-114413

AMES HEAT PIPE EXPERIMENT (AHPE) EXPERIMENT DESCRIPTION DOCUMENT

JANUARY 1972

TRW DOCUMENT NO. 13111-6033-R0-00

PREPARED BY

B. D. MARCUS

CONTRACT NO. NAS 2-5503

PREPARED FOR

NASA—AMES RESEARCH CENTER
MOFFET FIELD, CALIFORNIA 93405

MATERIALS SCIENCE STAFF

TRW
SYSTEMS GROUP

FOREWORD

The work described in this report was performed under NASA contract NAS 2-5503, "Design, Fabrication, and Testing of a Variable Conductance Constant Temperature Heat Pipe." The contract is administered by Ames Research Center, Moffett Field, California, with Mr. J. P. Kirkpatrick serving as NASA Program Manager.

The program is being conducted by TRW Systems Group of TRW Inc., Redondo Beach, California, with Dr. Bruce D. Marcus serving as Program Manager and Principal Investigator. Many persons contributed to the effort described in this report. However, special acknowledgement should be given to Mr. G. L. Fleischman, Mr. J. P. Kirkpatrick, Mr. O. W. Clausen, Mr. B. B. Harmel and Professor D. K. Edwards for their contributions in the design and test phases, as well as Mr. V. H. Reineking and Mr. R. S. Boehnlein for their roles in the manufacture of the hardware.

TABLE OF CONTENTS

FIGURES

TABLES

1.0 INTRODUCTION

A gas-controlled variable conductance heat pipe, designated the Ames Heat Pipe Experiment (AHPE), has been qualified for flight aboard the Orbiting Astronomical Observatory (OAO-C).

The primary objectives of this experiment were to (1) determine the performance and reliability of a variable conductance heat pipe in the zero-g, vacuum environment of space, and (2) demonstrate in a specific engineering application the effectiveness of a variable conductance heat pipe in providing temperature stability for spacecraft equipment which experiences varying electronic duty cycles and changing thermal boundary conditions.

A summary of the heat pipe design and the qualification and flight acceptance test program has been previously published [1]. The analytical techniques and ancillary experiments utilized in arriving at the ultimate system design have also been published elsewhere [2,3,4,5]. It is the purpose of this document to provide a more in-depth discussion of the system design and a detailed description of the AHPE hardware.

2.0 OAO-C FLIGHT OPPORTUNITY AND CONSTRAINTS

The functional role of the variable conductance heat pipe/radiator, officially entitled "The Ames Heat-Pipe Experiment" (AHPE), is to provide temperature control for the OAO-C spacecraft's On-Board Processor (OBP) by regulating the heat transfer from the back of the OBP honeycomb equipment shelf to space (Figure 1). Power dissipation from the OBP varies from about 10 to 30W and the energy incident on the Alzak-coated radiator (α/ϵ = 0.17/0.75) varies as shown in Table I. The radiator receives no direct insolation and the large amount of incident infrared energy is emitted from a nearby solar cell panel. It will be shown later that this large infrared flux was a dominant factor in the AHPE design.

Without the AHPE, the conventional use of thermostatically controlled heaters and radiative coupling to space would result in an OBP platform temperature fluctuation from 0° to 140°F. Since the AHPE is an experiment, a major constraint was that, for any AHPE failure mode, the temperature of the OBP would not exceed these limits. This required a radiative heat-transfer path parallel to the AHPE which, at 30W dissipation on the platform, allows only 22W to be conducted through the heat pipe. Six watts are radiated directly to the radiator, and 2W are radiated to the surrounding walls. Therefore, an AHPE performance goal was established to maintain the pipe's mating surface with the OBP platform at a nominal 65 $\pm$ 5°F, for changes from minimum to maximum incident fluxes, and for power variations through the heat pipe up to a maximum of 22W. Special concern for the minimum power through the heat pipe (at full-off conditions) was not warranted due to the large amount of heat (about 8W) being lost through the parallel radiative coupling.

Additional constraints were (1) the available volumetric envelope of 28 X 16 X 3-1/2 inches; (2) a requirement for meaningful testing in the earth's gravitational field; and (3) a schedule delivery 11 months after contract go-ahead.

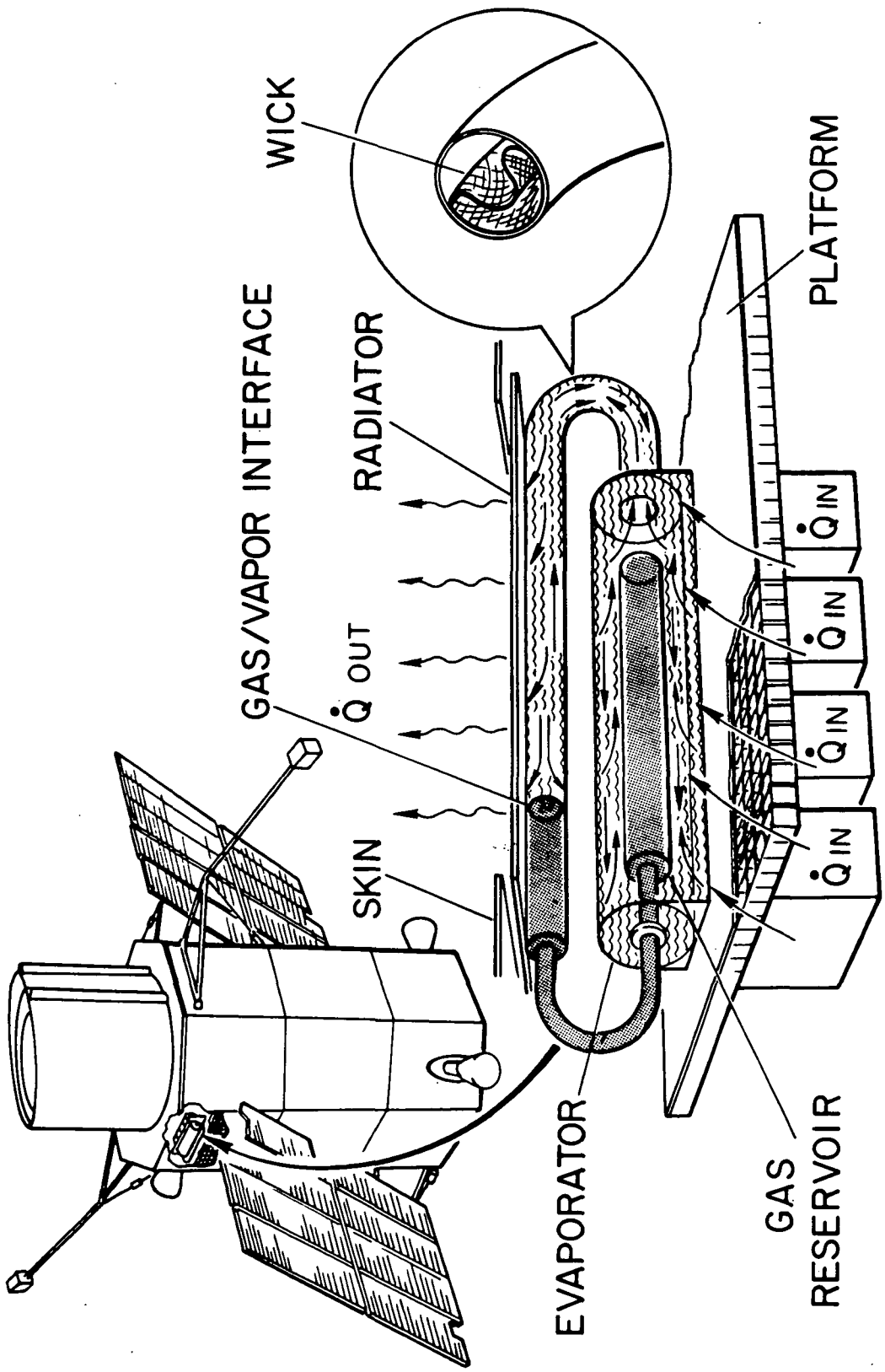

Figure 1. Ames Heat Pipe Experiment (AHPE) on OAO-C

TABLE I

INCIDENT FLUXES ON AHPE RADIATOR*

	SOLAR	INFRARED		
	ALBEDO	EARTH	PANEL	TOTAL IR
MAX	15.96	16.75	43.23	59.98
MIN	7.22	10.24	14.87	25.11

* Orbital average (Btu/hr-ft^2)

3.0 THERMAL DESIGN

3.1 Preliminary Control Analysis - Selection of Reservoir Configuration and Working Fluid

The AHPE performance goals call for rather close control of the evaporator temperature ($\pm$ 5°F) where the thermal environment both inside and outside of the spacecraft varies substantially. Because the operating temperature of a gas-controlled heat pipe varies with reservoir temperature, and because there was no constant-temperature position in the OBP bay at which to mount the reservoir, a design analysis was performed for the two locations where its temperature could be determined. In one case (cold reservoir) the reservoir is located at the end of the condenser, so that its temperature depends on the effective space temperature (T_s) and fluctuates with variations in thermal environment. The second case (hot reservoir) places the reservoir inside the evaporator, so that its temperature range corresponds to the heat pipe's control range.

There exists a fundamental difference in these two approaches. The cold external reservoir must be wicked, or else vapor diffusing through the gas will condense in the reservoir and be lost to the wicking system. The partial pressure of vapor in the reservoir will then be the vapor pressure corresponding to its temperature.

On the other hand, the hot internal reservoir must not be wicked, for its vapor pressure would then be equal to that in the evaporator (i.e., the total pressure) and it could contain no gas. Without wicking, the partial pressure of vapor in the reservoir is established by diffusion to and from the reservoir entrance (e.g., the end of the condenser) and hence, at steady state conditions, corresponds to the temperature at this point.

The basic principle in designing a gas reservoir for a desired control range is that the molar gas inventory in a given heat pipe remains constant for all operating conditions. Assuming an ideal gas mixture, the molar inventory for an element of pipe volume is simply:

$$dn = \frac{P_g}{R_u T_g} dV \qquad (3\text{-}1)$$

where:

dn - number of moles of gas in the volume element dV

P_g - partial pressure of gas in dV

T_g - temperature of gas in dV

R_u - universal gas constant

Thus, for any given operating condition, one can obtain a value for the total molar inventory in the heat pipe by integrating Equation (3-1) over its volume. To size the gas reservoir, such expressions are written for the two operating extremes; i.e., the full-on condenser at maximum thermal boundary conditions and the full-off condenser at minimum thermal boundary conditions, without specifying the reservoir volume. These expressions are then solved simultaneously for the molar inventory and reservoir volume, other pipe parameters being specified.

Using this approach, a parametric "flat-front"* analysis was performed for preliminary AHPE specifications, comparing cold external vs. hot internal reservoirs for ammonia and methanol working fluids. The calculations were performed for several possible combinations of maximum and minimum radiator effective space temperature (T_s) which might be obtained using various coatings on the back of the radiator, and Alzak or second surface mirrors on its heat rejecting surface. The results are shown in Figures 2 and 3 for the cases where the back of an Alzak radiator is painted black ($-60 < T_s < -2°F$) and aluminized ($-107 < T_s < -19°F$), and for the case of a second surface mirror radiator with the back aluminized ($-110 < T_s < -24°F$). Figure 2 presents the results for methanol and Figure 3 for ammonia as the working fluid.

The curves, which represent the required reservoir-to-condenser volume ratio (V_R/V_c) to achieve a particular evaporator control range

* neglecting axial heat conduction and mass diffusion.

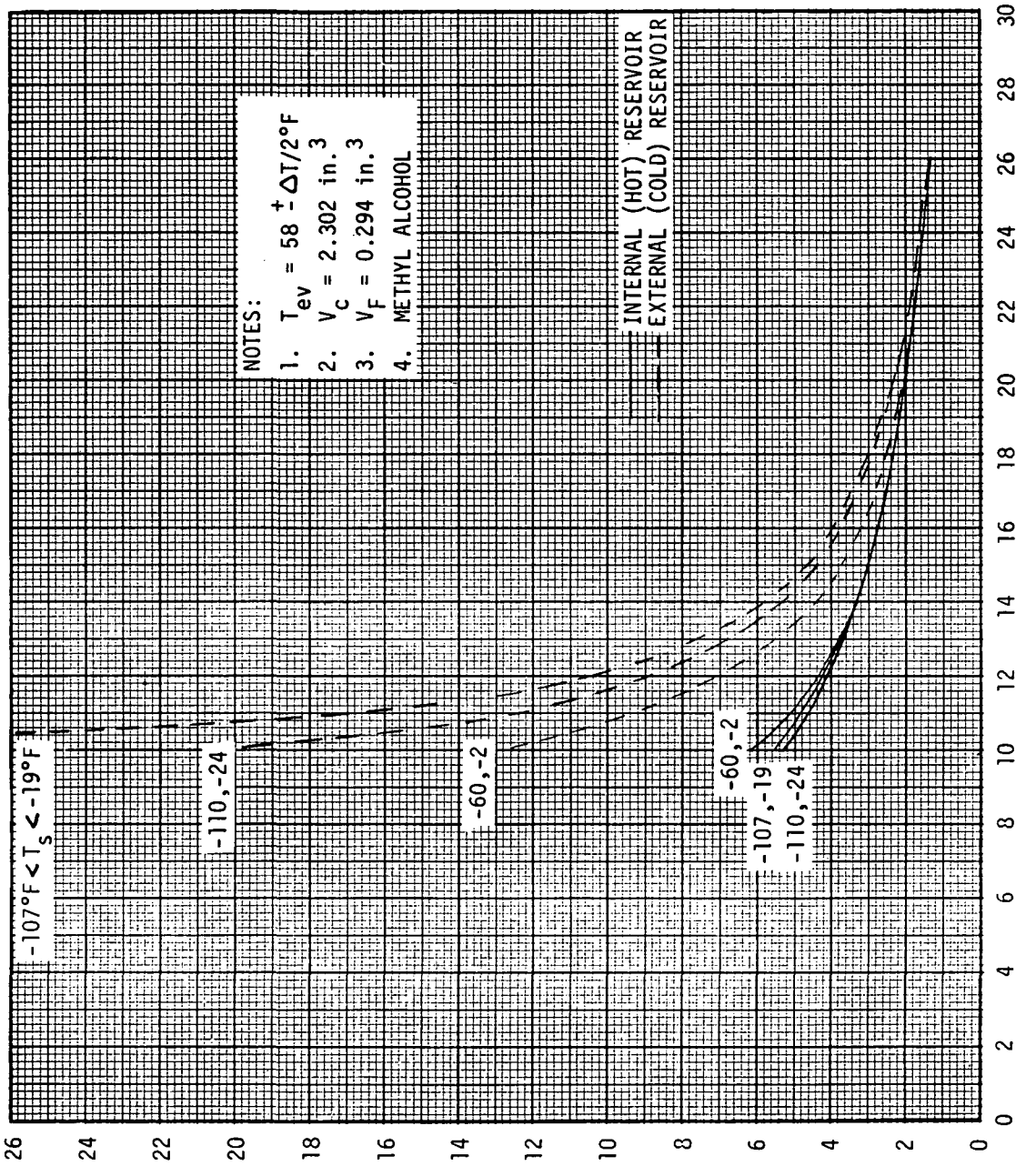

Figure 2. Volume Requirements for Hot and Cold Reservoirs - Methanol

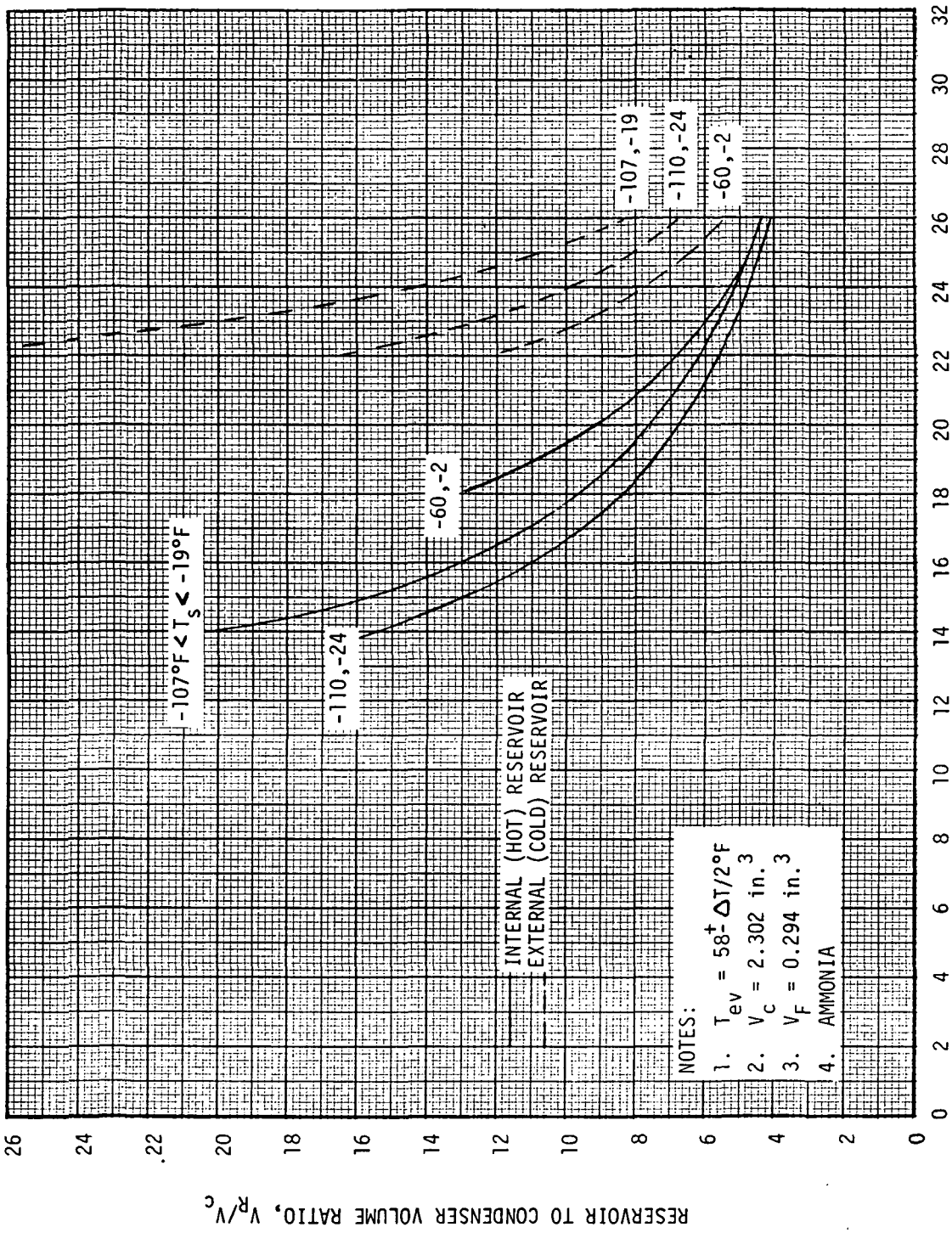

Figure 3. Volume Requirements for Hot and Cold Reservoirs - Ammonia

for the specified conditions, show several interesting features: (1) for either working fluid, the internal hot reservoir allows much closer control than the external cold reservoir, and (2) for either reservoir design, methanol allows much closer control than does ammonia.

This behavior becomes clear when one considers the way in which sink-temperature variations affect control. As shown by Marcus and Fleischman [2], the heat-pipe operating temperature is affected by changes in the reservoir gas temperature, and by variations in the partial pressure of vapor in the reservoir compared with the total pressure in the system. Thus, since the hot reservoir design minimizes reservoir-gas temperature fluctuations, it offers superior control. Also, for a given design approach, methanol offers better control because the change in vapor pressure over the specified ranges in effective space conditions is smaller compared with the total system pressure than for ammonia.

The results of Figure 3 indicated that it was not practical to obtain the desired $\pm$ 5°F control range (ΔT = 10°F) using ammonia, the preferred fluid from a hydrodynamic point of view. Furthermore, even using methanol (the second best hydrodynamic fluid), it appeared that the only practical approach to achieving the desired control range was to use a hot reservoir design. Thus, a hot internal reservoir pipe with methanol as the working fluid was selected for the AHPE.

It is also apparent from Figure 2 that superior control could be achieved with the back of the radiator aluminized. Because of the "non-interference" constraint on the experiment, it was not possible to aluminize the back of the entire radiator since a parallel radiation heat transfer mode was required between it and the OBP platform. However, it was feasible to insulate the back of a small portion of the radiator (3 inches) at the end of the condenser. This section would then act as a "cold trap", lowering the temperature at the entrance to the reservoir feed tube and hence the partial pressure of vapor in the reservoir. With this approach, superior control could be achieved with minimal impact on the non-interference constraint.

3.2 Final Control Analysis - Sizing the Reservoir

To actually size the reservoir for the OAO-C experiment, the procedure described earlier was repeated once all aspects of the design were iterated with each other and final specifications were established for the nominal operating temperature (65°F) , condenser size, vapor flow area, cold trap length, desired gas front travel, etc. These results are shown on Figure 4 for an Alzak radiator with and without a cold trap.

Using Figure 4 and available standard tube sizes from manufacturers' catalogs, a 7/8 in. O.D. X 0.016 in. thick tube was chosen for the reservoir. This yielded a reservoir/condenser volume ratio of 9.6 and a predicted control range of 6.4°F for the cold-trapped radiator.

This prediction, however, was based on the "flat-front" model for gas-loaded heat pipes (see Reference [4]). This model assumes that the interface between the active and inactive portions of the condenser is very sharp, and that axial conduction in the pipe wall and radiator is negligible. Thus, the analysis presumes that the temperature in the "shut-off" portion of the condenser is everywhere equal to the effective sink temperature.

These assumptions are actually not very good. Marcus and Fleischman [2] have shown that axial conduction is not negligible and leads to considerable spreading of the vapor-gas front. If, under conditions of higher condenser utilization, this causes the temperature at the end of the condenser ($T_{s'}$) to rise above the sink temperature ($T_{s'} > T_s$), the partial pressure of the vapor in a hot reservoir increases, causing an increase in operating temperature of the pipe and a widening of the control range.

Since these effects are quantitative rather than qualitative, the simple flat-front model does permit useful preliminary design analyses and trade-offs as described previously. However, it was necessary to treat the problem more rigorously. This was especially true for the AHPE in that, because of envelope constraints and active radiator-area requirements, only about three inches at the end of the

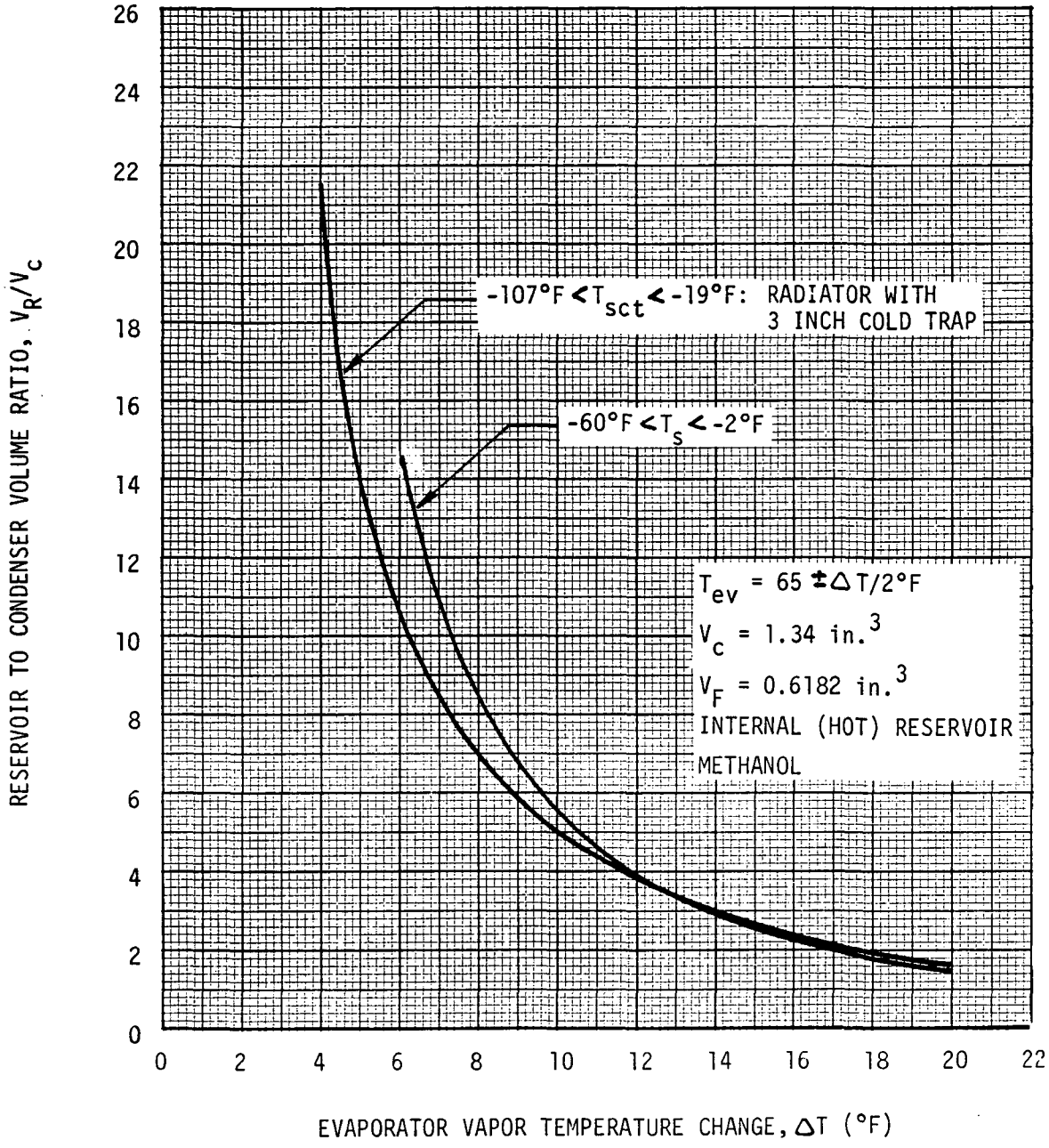

Figure 4. Volume Requirements for Hot Reservoir Methanol AHPE With and Without Cold Trap

condenser were available to develop the vapor-gas front and drop the temperature at the reservoir entrance ($T_{s,}$) low enough to minimize the partial pressure of vapor in the hot reservoir. To accomplish this, an analysis was formulated, based on a one-dimensional model which included (1) radiation to and from the finned condenser, (2) axial conduction in the walls, fins and wicks, (3) binary mass diffusion between the vapor and gas, and (4) an approximate treatment of wick resistance which is accurate for high conductance wicks. The governing equations were programmed for numerical solution on a digital computer.

This analysis and numerical solution are beyond the scope of this report and were reported elsewhere [5,6]. However, the results of its application to the AHPE design are discussed below.

The principal objective of applying the gas-front computer program to the design of the AHPE was to determine conditions for which the gas front could be formed over the length available.

A radiator optimization analysis was performed by NASA-ARC personnel indicating that 23.5 inches of a 26.5 inch total available length was required to be active in order to dissipate maximum power at minimum boundary conditions. Thus, only three inches of condenser length were available to form the gas front.

By using the gas front program to study the problem parametrically, it was found that the key variable affecting the length of the gas front, which was not constrained by other design considerations, was the axial conductance of the condenser tube and radiator fin. The effect of axial conductance on the calculated performance of the AHPE is shown in Figure 5. This graph shows the variation of two parameters as a function of the effective axial thermal conductivity (total axial conductance referenced to the cross-sectional tube wall area). The left-hand ordinate represents the equilibrium temperature ($T_{s,}$) at the entrance to the reservoir (end of the condenser) for full power at maximum boundary conditions. Thus, one sees that, even for relatively small values of k_{eff}, axial conduction causes the temperature at this point to rise above sink conditions; i.e., the front does not fully develop in three inches.

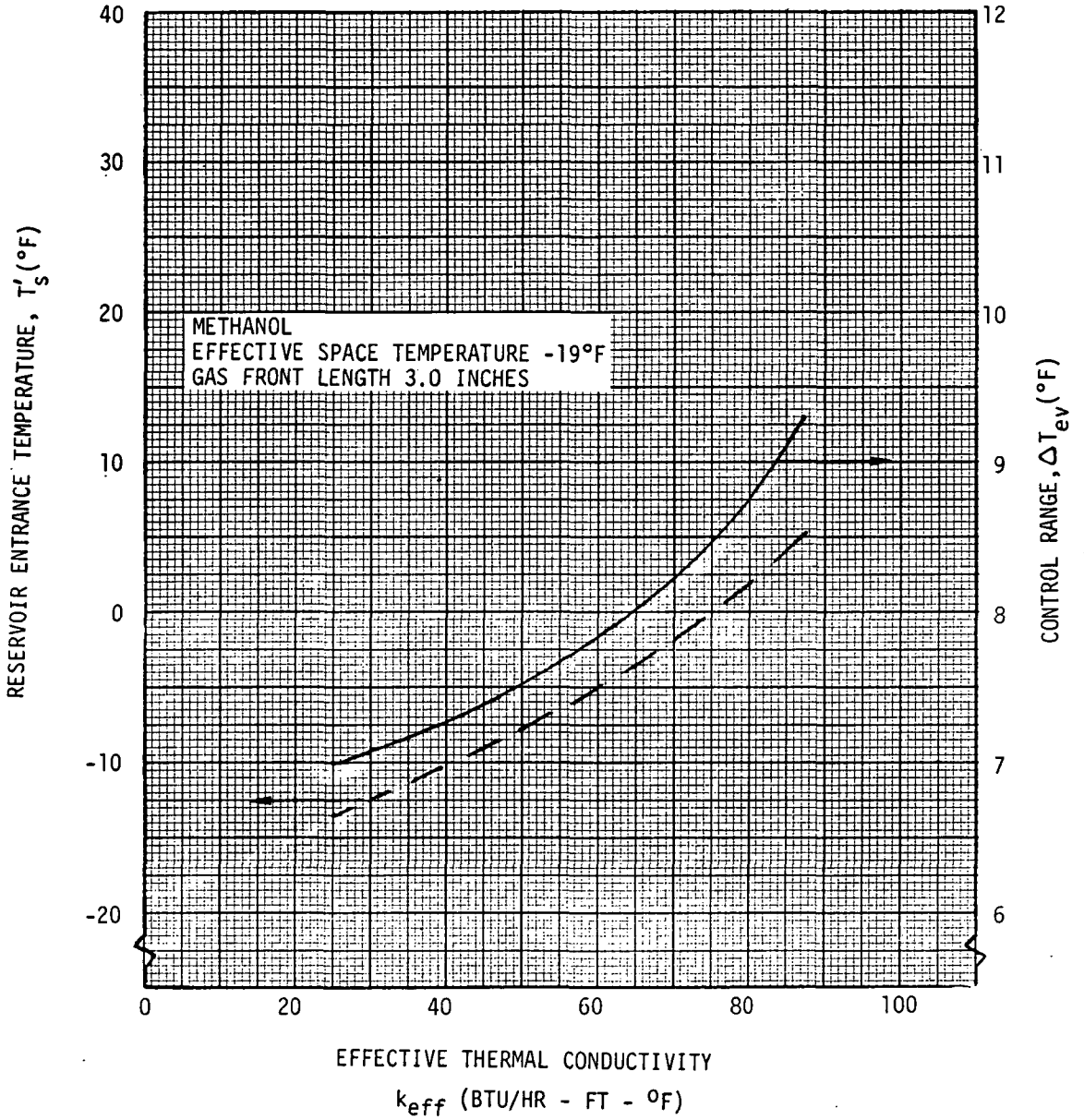

Figure 5. Effect of Axial Conductivity on Control Range and Reservoir - Entrance Temperature

As stated previously, the effect of this on hot reservoir pipes is to increase the partial pressure of vapor in the reservoir and widen the control range. This is clearly seen on the right-hand ordinate of the curve, which represents the variation in evaporator vapor temperature (ΔT_{ev}) between operating extremes of the heat pipe. As axial conductance increases, T_s, increases which results in a broader control range (ΔT_{ev}).

These calculations led to the conclusion that relatively small values of k_{eff} were required to achieve the desired control range. To accomplish this it was necessary to segment the radiator by constructing it of individual fins so that its conductance was anisotropic. That is, it had a high conductance perpendicular to the condenser tube, to yield a high radiator effectiveness, but a low conductance in the axial direction.

To further lower axial conductance, the condenser tube wall was machined to 0.016 inch thickness at the gaps between each segment. The initial wall thickness was 0.035 inches, which was necessary to bend the condenser tube 180° within the allowed 3-1/2 inch envelope without buckling.

A non-segmented radiator of the size used would have a k_{eff} on the order of 2000 Btu/hr-ft-°F. By designing the last three inches of the radiator with 0.5-inch fins and 0.150-inch gaps at their roots, it was possible to reduce k_{eff} to 41.3 Btu/hr-ft-°F in this critical region and establish an anticipated control range of 7.3°F.

This range, however, is that of the evaporator vapor temperature. To it must be added the range of temperature drop into the evaporator (1.3°F). Thus, the total predicted variation in the saddle interface temperature was 8.6°, slightly better than the design goal of 10°F.

3.3 Diffusion-Controlled Transients

The selection of a hot, non-wicked reservoir involved a trade-off in terms of transient performance. Because the partial pressure of vapor within the reservoir is established by diffusion of vapor to and

from the reservoir entrance, any changes in this parameter occur relatively slowly. This phenomenon was studied in some detail and has been reported elsewhere [2,3]. In order to estimate the diffusion-dominated transient response of the AHPE, a simplified one-dimensional, quasi-steady-state analysis was performed. This analysis (Appendix A) served to generate the following order-of-magnitude expression for the diffusion time constant which characterizes this process.

$$\tau_{\mathcal{D}} = \left[\frac{V_R L_F}{A_F} + \frac{(L_R^2 + L_F^2)}{2} \right] \frac{1}{\mathcal{D}_{vg}} \qquad (3\text{-}2)$$

where:

V_R - volume of reservoir

A_F - flow area of feed tube

L_F - length of feed tube

L_R - length of reservoir

$\mathcal{D}_{vg}$ - mass diffusivity for vapor-gas pair

Equation (3-2) showed that to maximize the heat pipe response to diffusion-dominated transients, one should minimize the length and maximize the diameter (flow area) of the reservoir feed tube. This was attempted in the AHPE design, leading to the following parameters for Equation (3-2).

$V_R = 7.44 \times 10^{-3}$ ft^3

$A_F = 6.42 \times 10^{-4}$ ft^2

$L_F = 0.417$ ft

$L_R = 1.96$ ft

$\mathcal{D}_{vg} = 3.06$ ft^2/hr *

$\tau_{\mathcal{D}} = 2.21$ hrs

* The binary diffusion coefficient between methanol and nitrogen was not available in the literature and had to be calculated from first principles. This calculation is presented in Appendix B.

Experiments on the prototype unit, in which the heat pipe was overdriven (forcing vapor into the reservoir) and allowed to recover, substantiated this predicted transient response.

3.4 Start-up with Liquid in the Reservoir

It has been experimentally demonstrated that the presence of liquid in the gas reservoir of a hot reservoir heat pipe gives rise to high pressure and temperature transients when the pipe is started [2,4]. This is caused by the liquid in the hot reservoir vaporizing and displacing the gas.

An upper bound for this phenomenon occurs when all the gas is forced into the condenser. A quantitative estimate for this condition can be obtained using the "flat-front" analysis discussed in Reference [4, page 191]. The results of such an analysis for the AHPE design are shown in Figure 6. Evaporator temperature and pressure are plotted as functions of the input power to the heat pipe for start-up under maximum (T_s = -2°F) and minimum (T_s = -60°F) effective space temperatures.

It is apparent from Figure 6 that a transient over-pressure of as much as 11 times the nominal design pressure (1.95 psia at 70°F) could result from a start-up with liquid in the reservoir. In the AHPE, these pressures pose no problem. However, this phenomenon would certainly be troublesome with an ammonia heat pipe, in which the vapor pressure would be 129 psia at 70°F.

Any liquid in the reservoir will slowly diffuse out due to the gradient in mole fraction of vapor between the hot reservoir and its cold entrance. Thus, the heat pipe will automatically "rectify" itself. However, the rectification process occurs by diffusion and is relatively slow. Thus, to minimize such effects on the AHPE, the design included a perforated Teflon plug blocking the entrance to the reservoir, which serves to impede liquid from entering the reservoir while permitting the gas to pass freely. The plug was 0.215 inches in diameter and 0.0625 inches thick, with eighty 0.009 inch diameter holes drilled through it.

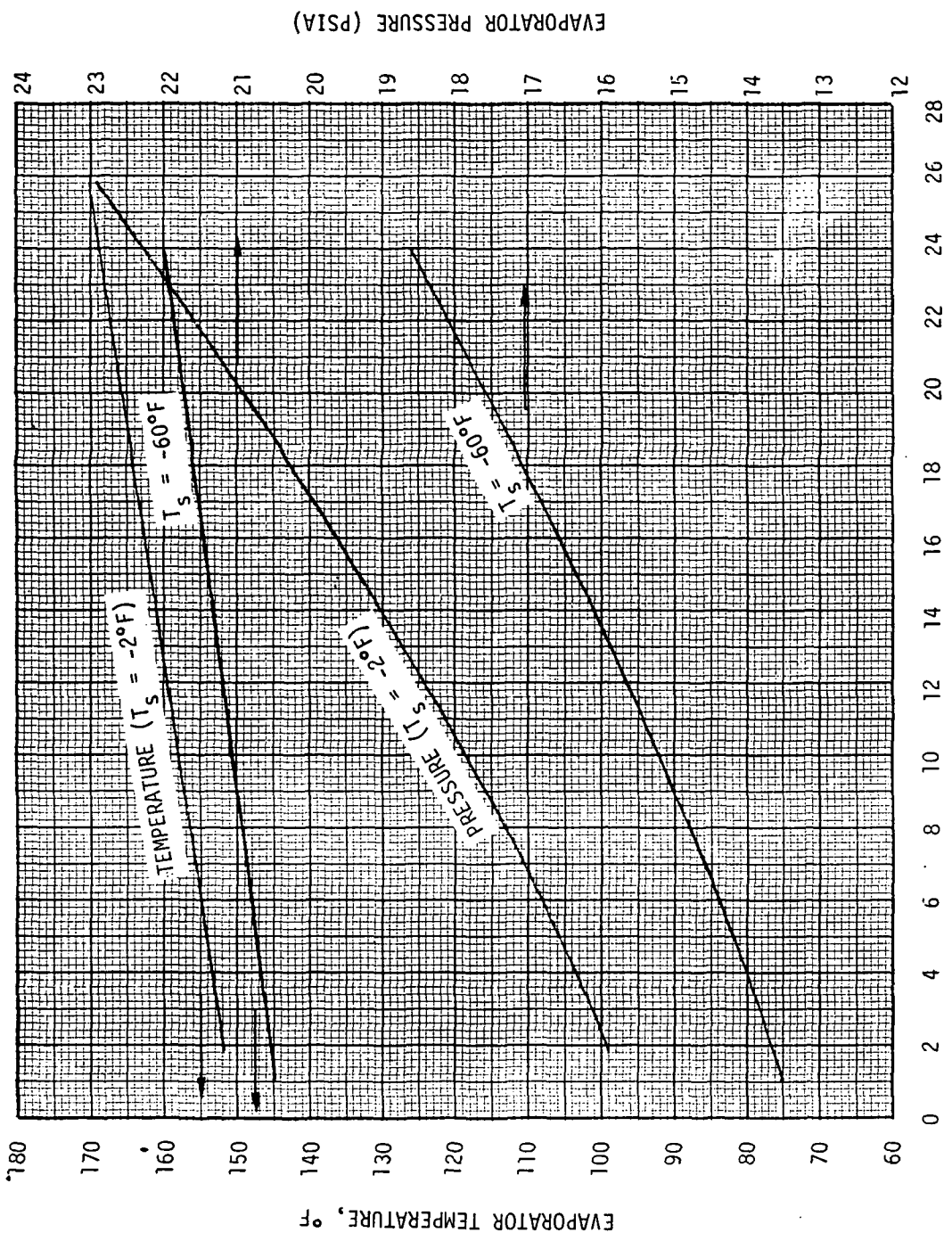

Figure 6. Maximum Evaporator Pressure and Temperature With Liquid in the Reservoir

3.5 Hydrodynamics

The hydrodynamic design of the AHPE evolved through multiple iterations of the pertinent factors, resulting in the hardware configuration shown schematically in Figure 7. A summary of design features and the considerations leading to their selection follows.

Water, ammonia and methanol were considered as potential working fluids for the AHPE. Although water is superior from both hydrodynamic [Reference 3, page 84] and control [Reference 4, pages 107 and 110] points of view, it was rejected because of its high freezing point and incompatibility with the preferred materials of construction. The choice of methanol over ammonia was made on the basis of the required control range. Although ammonia is a superior fluid hydrodynamically, it could not meet the 65 $\pm$ 5°F requirement using passive control techniques.

For maximum reliability of the AHPE, a conventional homogeneous type wick structure was preferred. Thus, preliminary design efforts were directed toward the development of an optimum wick to handle the heat load requirements (24 watts) without the use of arteries. Moreover, attention was primarily focused on wire mesh wicking because of (1) its availability in a wide range of pore sizes, (2) relative ease of manufacture, and (3) the availability of substantial experimental data and successful correlations for wick properties. The last factor allowed for analytical design and optimization of the wicking system. This procedure has been documented elsewhere [Reference 3, pages 37 through 57] and will not be repeated here except for the resulting equation for the optimum mesh wire spacing.

$$\delta_{opt} = \frac{4\sigma}{3S\Delta P_o} + 4\left[\frac{\sigma^2}{9S^2\Delta P_o^2} - \frac{\left(1-\frac{\pi F}{4}\right)}{3\pi FSM\Delta P_o}\right] \qquad (3\text{-}3)$$

where:

δ_{opt} - optimum wire spacing

σ - surface tension

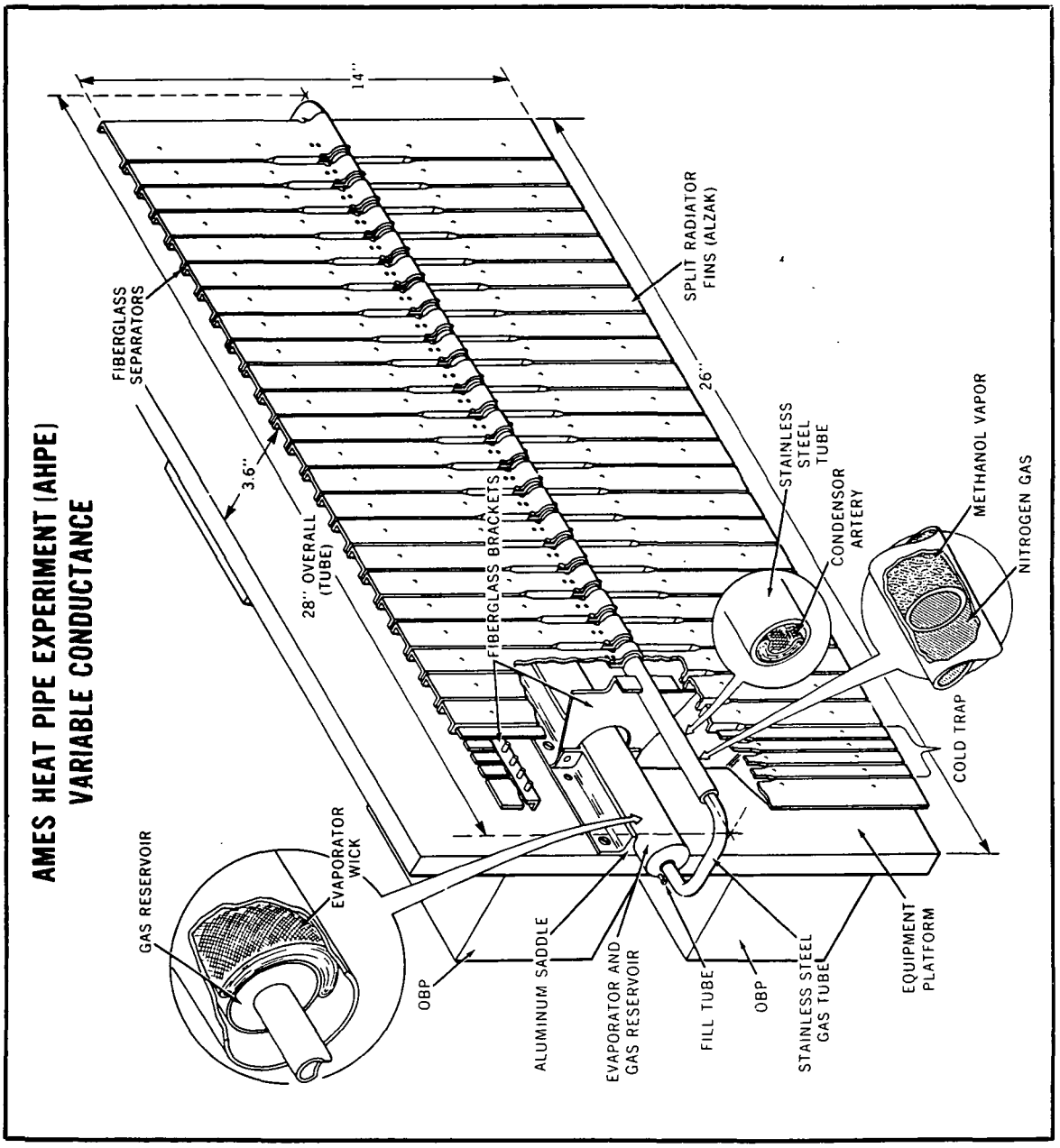

Figure 7. AHPE Hardware Configuration

S - safety factor

ΔP_o - wick loading - liquid pressure depression due to factors other than liquid flow losses through the section of wick under study

F - crimping factor for screen mesh

M - mesh size for screen - wires per inch

Equation (3-3) relates δ_{opt} to M, the screen mesh size. By plotting Equation (3-3) on a graph of δ, M couples for available screen meshes, the optimum wick, which corresponds to the screen of largest mesh size which falls on (or near) the curve, can be established for given values of S, ΔP_o, F($\approx$1.05) and σ.

The heat pipe had to operate in a 1-g as well as a 0-g field to permit testing. Since the optimum wick structure for a heat pipe is a function of the g-field in which it operates (it affects the body force term in ΔP_o), it was necessary to compromise 0-g capacity to provide sufficient 1-g capacity. Thus, Equation (3-3) was used to establish optimum wicks for both 0-g and 1-g environments and a compromise solution accepted.

Another factor constraining the wick design was that dimensional limitations required the pipe to be bent on a tight radius. This, and the desire to achieve a large reservoir-to-condenser volume ratio (9.6) with a reasonable reservoir volume, dictated a relatively small diameter thick-walled condenser tube (7/16" O.D. X 0.035" wall).

After optimal screens were determined for the evaporator and condenser sections, performance predictions for the AHPE were run utilizing a digital computer heat pipe performance program based on the analysis of [Reference 3, Section 3]. The results of these calculations showed that, even with optimal wicks, conventional screen wicks could not meet the performance requirements. The combination of a small available wick flow area and a relatively poor working fluid (from a hydrodynamic point of view) resulted in excessive liquid pressure drops in the condenser and adiabatic sections of the pipe. As a consequence, it was necessary to

utilize arteries in the condenser wick design.

Several types of arteries were considered, but the need for the artery to maintain its integrity when bent on a tight radius reduced the choice to two preferred configurations as shown on Figure 8.

Figure 8a depicts a multiple channel artery made up of 94 mesh screen with four 9 mil gaps. The wick is made by spot-welding (or sewing) 9 mil spacer wires to (or through) a strip of screen and then winding the screen in spiral fashion. The four channels provide low resistance flow paths and the 94 mesh overwrap establishes the maximum capillary head for the condenser and adiabatic sections.

Figure 8b shows a "filled" artery consisting of six strips of 40 mesh screen wrapped in a double layer of 94 mesh screen. In this case, the 40 mesh layers provide the low resistance flow path and again the 94 mesh overwrap establishes the maximum capillary head.

Both the 9 mil gap width and the 40 mesh internal fill were established to assure self-priming of the arteries in a 1-g field. The 94 mesh overwrap was sized to yield maximum parallel axial flow.

Both of these artery configurations offered sufficient flow capacity to meet the design requirements. Configuration "a" yielded slightly greater capacity than "b", but was more difficult to manufacture and maintain dimensional control. Consequently, the filled artery was selected for the final design.

Because the heat pipe contains a non-condensible gas, which tends to promote nucleation in a superheated liquid, it was decided not to use arteries in the evaporator. Even though calculations indicated that nucleation would not occur at the anticipated superheat levels, the margin of safety was not great enough to risk vapor blockage of an artery. Thus, the primary evaporator wick consisted of multiple layers of 145 mesh screen sintered to the pipe wall. As in previous calculations, the 145 mesh size was established through optimization with Equation (3-3).

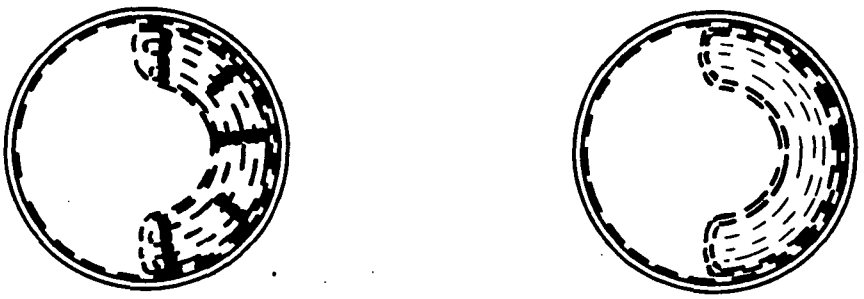

Figure 8. Preferred Condenser Artery Configurations: a) multiple channel spiral artery - screen wound around spacer wires; b) filled artery - fine screen wrapped over coarse screen.

The function of the artery in the condenser section is to de-couple the axial flow resistance from the capillary pumping head, providing higher flow capacities than can be achieved with homogeneous wicks. It is also desirable to de-couple the radial heat transfer and axial flow processes in order to achieve low temperature drops with thick wicks. Thus, in order to minimize the temperature drops due to heat transfer into and out of the device, and thereby to maximize full-on conductance, the primary wicks were designed to occupy only half the circumference of the pipe, as shown in Figures 7 and 8. A single layer of 150-mesh screen in the condenser and a double layer in the evaporator were provided to pump the liquid around the circumference of the pipe to and from the primary wicks carrying the axial flow. Heat transfer into and out of the pipe was principally through these thin wicks, which were sintered to the pipe wall to improve thermal conduction. A single layer of 150-mesh screen was also spotwelded to the outside surface of the gas reservoir in order to assure the presence of liquid to provide reservoir temperature control during cooling transients.

Figure 9 shows the estimated hydrodynamic performance of the AHPE at 70°F under a 24 watt load (worst case conditions).

The figure shows the pressure drops in the vapor core, primary wicks and thin circumferential wicks (ΔP between dashed and solid lines). The discontinuity in the vapor loss curve at the end of the evaporator is due to the reduction in flow area from the 1-1/4 inch diameter evaporator tube to the 7/16 inch diameter condenser tube. The discontinuity in slope of the liquid loss curve within the bend is due to a 1.5 inch section of homogeneous 94 mesh wick to seal the condenser artery. Note that the flow loss curves are straight lines within the bend section since there is no heat addition or removal in this region; i.e., it is an adiabatic section.

The gravity terms ΔP_g represent the head corresponding to the height of each section of the pipe above the lowest point of the system (bottom of the evaporator). This value represents the average integrated gravitational head over the wick flow area and is the appropriate value to be used for 1-g operation in the horizontal mode.

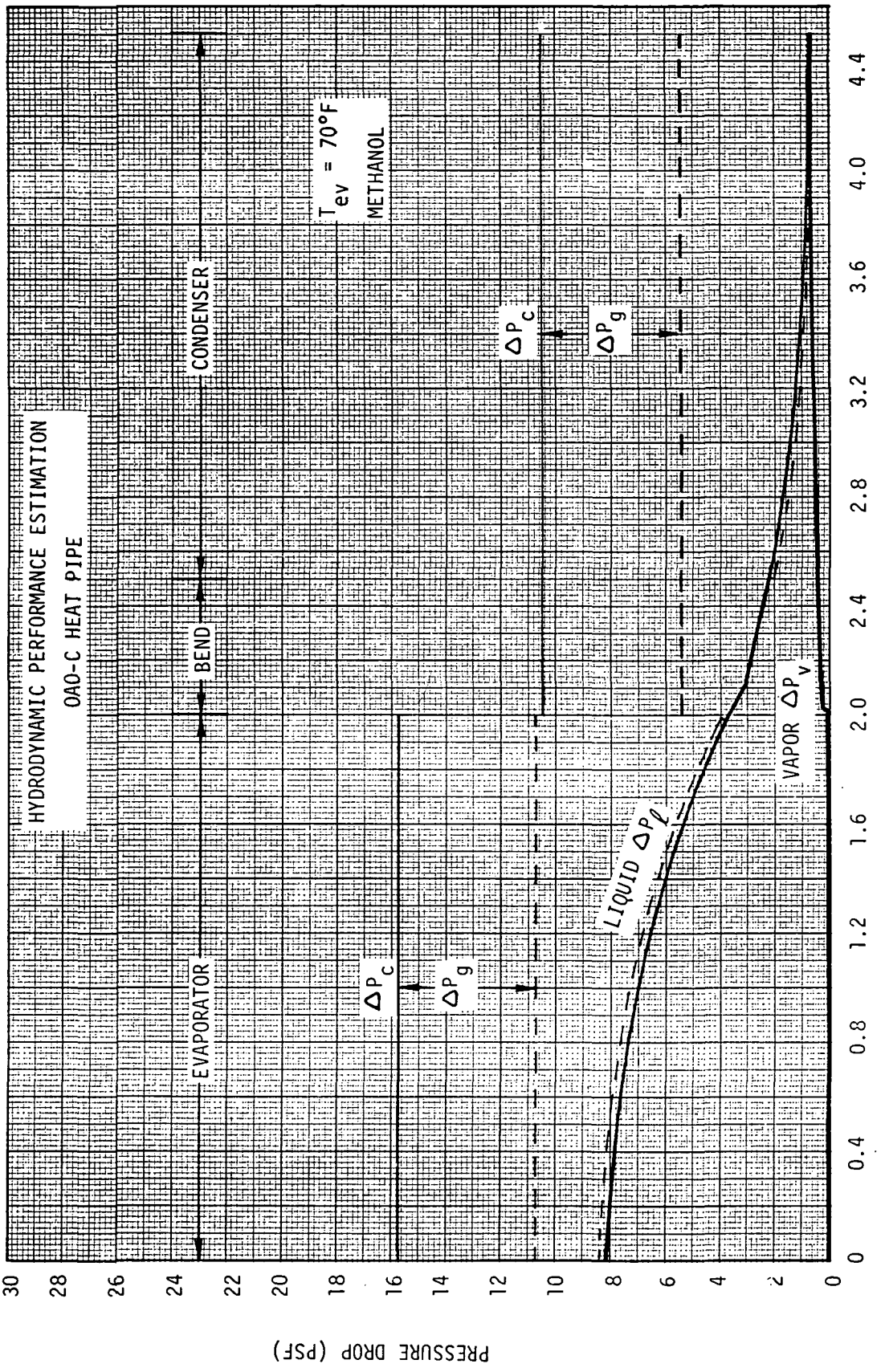

Figure 9. Pressure Drop Calculations for AHPE Hardware Under Worst Case Conditions

As seen in Figure 9, the maximum capillary head (ΔP_c) minus the gravitational head (ΔP_g) is everywhere greater than the liquid pressure depression ($\Delta P_\ell + \Delta P_v$), indicating successful operation of the heat pipe under these conditions. Further explanation of this analysis procedure will be found in [Reference 3].

The margin of safety for the AHPE under a 24 watt load over the anticipated operating temperature range is summarized in Table II:

TABLE II

SUMMARY OF HYDRODYNAMIC PERFORMANCE ESTIMATION
OAO-C CONSTANT TEMPERATURE HEAT PIPE

Temperature (°F)	Overall Safety Factor 0-g*	Overall Safety Factor 1-g**	Condenser Safety Factor 0-g*	Condenser Safety Factor 1-g**
60	1.82	1.16	2.98	1.76
65	1.87	1.18	3.05	1.77
70	1.92	1.20	3.12	1.78

* Safety Factor $= \dfrac{\Delta P_c}{\Delta P_\ell + \Delta P_v}$

** Safety Factor $= \dfrac{\Delta P_c}{\Delta P_\ell + \Delta P_v + \Delta P_g}$

3.6 Heat Transfer

Variation in Heat Pipe Conductance:

The fundamental purpose of the gas-loaded heat pipe is to passively vary the conductance between the heat source and sink. The overall conductance is, of course, not only that of the heat pipe, but also includes other thermal processes (radiation, conduction) coupling the source and sink. However, in terms of a heat pipe experiment, one is primarily concerned with the pipe conductance between the outside walls of the evaporator and condenser. This is defined by Equation (3-4):

$$C = \frac{q}{T_{w_e} - T_{w_c}} \qquad (3\text{-}4)$$

where:

C = pipe conductance

T_{w_e} = outside wall temperature of evaporator

T_{w_c} = outside wall temperature of condenser

q = heat transfer rate

At any given operating condition, the quantity $(T_{w_e} - T_{w_c})$ is made up of three components: (1) the temperature drop going into the evaporator, (2) the saturation temperature drop associated with the vapor flow loss, and (3) the temperature drop going out of the condenser.*

The temperature drops into the evaporator and out of the condenser themselves consist of two components; that by conduction through the wall and that through the wick.

---

* The temperature drops associated with the evaporation and condensation processes can generally be neglected.

To sum the various temperature drops, the following relationships apply:

$$\text{Conductance} = \frac{1}{\text{Resistance}} \qquad (3\text{-}5)$$

Resistance for conduction through thin cylinders:

$$R = \frac{t}{k_{eff} A}$$

where:

t = thickness

k_{eff} = effective thermal conductivity

A = heat flow area

Resistance of convective or boiling process:

$$R = \frac{1}{hA}$$

where:

h = coefficient of heat transfer

Condenser Conductance:

The condenser conductance is, of course, the variable quantity in a gas-controlled pipe. Its maximum value corresponds to the full-on condition and its minimum value to the full-off condition. The AHPE employs an asymmetrical wick in the condenser to partially de-couple the radial heat transfer and axial flow processes.

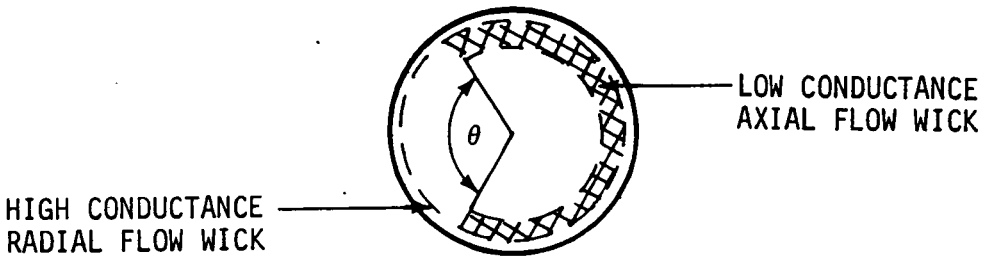

If one conservatively bases the conductance on heat transfer through the thin-wick section only, one obtains:

$$C_{cond\text{-}max} = \frac{1}{\left(\frac{t}{k\,A}\right)_{tube} + \left(\frac{t}{k_{eff}\,A}\right)_{wick}} \qquad (3\text{-}6)$$

where the areas used are $\theta/2\pi$ times the pertinent circumferential area.

In Equation (3-6), k_{eff} refers to the effective conductivity of the wick-fluid matrix. This is a difficult quantity to estimate for it depends on the relative thermal conductivities of the wick material and fluid, the geometry of the wick matrix, and the degree of bonding between the wick and tube wall.

However, experience has shown that for metal wicks which are simply held against the wall mechanically, the wick matrix contributes little to conduction other than to displace fluid and k_{eff} for low conductivity fluids is approximately given by:

$$k_{eff} = k_{liquid}/\phi \qquad (3\text{-}7)$$

where ϕ is the volumetric porosity.

If the wicks are sintered to the tube wall an improvement in k_{eff} is to be expected. However, the degree of improvement is a function of the type and thickness of the wick, and is not possible to predict with any accuracy.

The minimum condenser conductance refers to the full-off condition. However, this itself requires definition. At first glance, one might define the full-off case as that at which the beginning of the vapor-gas front coincides with the beginning of the radiator. According to TRW's gas-front program [5], this would yield a heat transfer rate through the pipe of about 7 Btu/hr for average boundary conditions.

It is not necessary, though, to insist that the front only move up to the start of the radiator at the full-off case. It can just as well be pushed back into the adiabatic section. In this case, heat transfer will be through the tube wall from the front to the radiator and will diminish as the front moves farther from the radiator. A worst case calculation for this is to determine the axial heat transfer in the tube for a 60°F operating temperature and a -60°F radiator (minimum boundary conditions) as a function of the distance from the front to the radiator. The results of such calculations are shown on Figure 10. From the figure it is seen that moving the front two inches past the radiator reduces the heat leak to about 0.55 watts ($\sim$ 1.9 Btu/hr) and that moving it back further does not offer very rapid improvement.

This calculation, of course, assumes that a front exists for all these conditions. This may not be the case for very low power rates. However, if a front does not form, an upper bound on the heat leak can be determined from the mass diffusion rate of vapor across the adiabatic section plus conduction through the wall. This is given approximately by:

$$q = \dot{m}\,\lambda = -\mathcal{D}_{vg}\,\frac{d\rho_v}{dz}\,A_v\,\lambda + k_t\,A_t\,\frac{dT}{dz} \qquad (3\text{-}8)$$

where:

q = heat leak

$\mathscr{D}_{vg}$ = diffusivity of vapor-gas pair

ρ_v = vapor density

A_v = vapor flow area

λ = latent heat of vaporization

k_t = thermal conductivity of tube wall

A_t = tube wall cross-sectional area

T = temperature

z = axial dimension

For the AHPE design, Equation (3-8) yields a heat leak of 0.63 Btu/hr.

To summarize these results, it appears that the heat transfer at the full-off condition is a maximum of 7 Btu/hr if the front is right at the beginning of the radiator, and a minimum of 0.6 Btu/hr if no front forms at all. If a front exists in the adiabatic section, an upper bound of the heat transfer is given by Figure 10. To express these results in terms of conductances, one simply divides the heat transfer by the temperature potential.

Evaporator Conductance:

If radial heat transfer in the evaporator is by conduction as in the condenser, the conductance is again given by Equation (3-6). However, it is frequently the case in low temperature heat pipes that heat transfer in the evaporator involves vapor generation within the wick (by boiling or internal surface evaporation). In this case, the term $(\frac{t}{k_{eff}\, A})_{wick}$ in Equation (3-6) must be replaced by $(\frac{1}{h\, A})$ where h is the coefficient of heat transfer characterizing the process. In all cases this improves

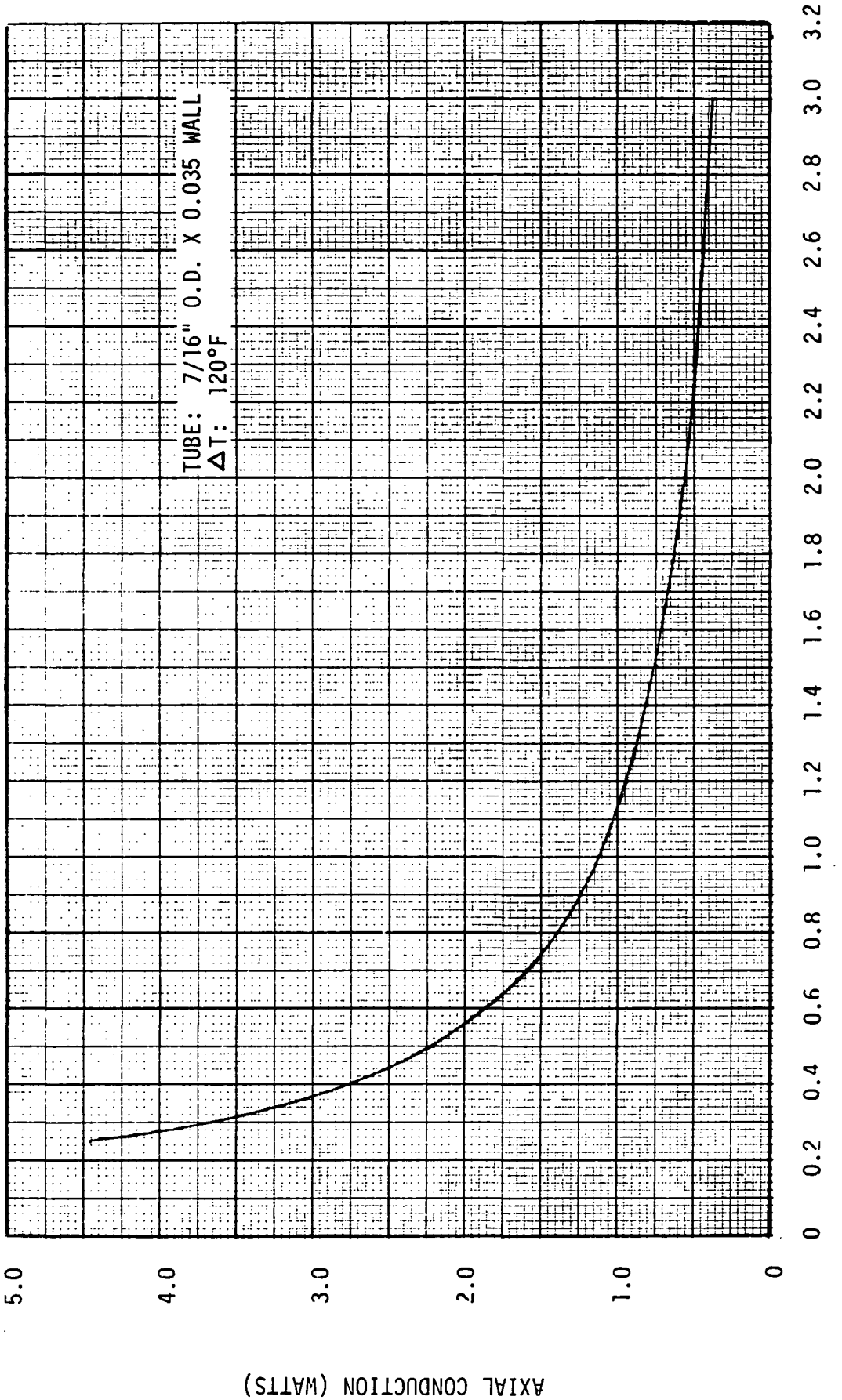

Figure 10. Axial Heat Conduction in Adiabatic Section from Vapor-Gas Front to Radiator: Full-Off Condition

the conductance, but at the expense of interference with the liquid hydrodynamics.

The AHPE has been designed to operate in the conduction mode to increase confidence in the design calculations (see Nucleation Criterion for Evaporator).

A summary of calculated values for conductances and temperature drops in the OAO-C heat pipes is presented in Table III:

TABLE III

CALCULATED CONDUCTANCES AND TEMPERATURE DROPS

	Full-on	Full-off
Heat Transfer Rate Btu/hr	82	1.9
Condenser Conductance Btu/°F-hr	38	.016
Condenser ΔT °F	2.16	120
Vapor Flow Loss °F	.06	~ 0
Evaporator Conductance Btu/hr-°F	63	63
Evaporator ΔT °F	1.3	.03
Over-all ΔT °F	3.52	120
Over-all Conductance Btu/°F-hr	23.3	.016

Nucleation Criterion for Evaporator:

Although the evaporator wick does not contain an artery and, hence, can sustain boiling to some extent, it is preferable to avoid this for it invalidates the hydrodynamic calculations which are based on fully saturated wicks. Thus, it is necessary to assure that the conduction temperature drop across the evaporator wick does not exceed the critical superheat for nucleation of the working fluid at the wall.

This critical superheat is given by [Reference 3]:

$$\Delta T_{crit} = \frac{T_{sat}}{J\lambda\rho_v}\left[\frac{2\sigma}{r_n} - \Delta P_c^*\right] \qquad (3\text{-}9)$$

where:

T_{sat} = saturation temperature of fluid

σ = surface tension

J = mechanical equivalent of heat

λ = latent heat of vaporization

ρ_v = density of vapor

r_n = radius of critical nucleation cavity

ΔP_c^* = maximum value of capillary head along the evaporator

All of the terms in Equation (3-9) are known except r_n, which is a function of the surface finish. For typical engineering surfaces used in pool boiling, r_n varies between 10^{-4} and 10^{-3} inches. For the AHPE operating at 65°F and maximum load, Equation (3-9) yields the following range of critical superheat values:

$r_n = 10^{-3}$ in. $\quad \Delta T_{crit} = 3.5°F$

$r_n = 10^{-4}$ in. $\quad \Delta T_{crit} = 51°F$

This is to be compared with a conservatively* calculated value of 1.3°F for the actual temperature drop across the two layers of 150 mesh screen in the heat input region of the evaporator. Thus, there would appear to be a safety factor of at least about 2.5 assuring an absence of ebullition.

One must, however, use care in accepting these results since the applicable range of r_n values was extracted from pool boiling literature for smooth surfaces. The presence of the wick on the surface could substantially alter this. To examine whether this might represent a problem, one can first calculate the critical nucleus assuming that cavities of all sizes were present. This can be done using the nucleation theory of Rohsenow and Bergles [6]. Their equation for the critical radius is:

$$r_n = \left[\frac{2\sigma \, T_{sat} \, k \, V_{\ell g}}{\lambda \, (q/A)} \right]^{1/2} \qquad (3\text{-}10)$$

where:

- k - thermal conductivity
- $V_{\ell g}$ - difference in specific volumes of vapor and liquid
- (q/A) - radial heat flux into evaporator

For the AHPE at maximum load, Equation (3-10) yields:

r_n = 0.0055 in.

This result implies that, were a nucleation cavity with radius 0.0055 in. present on the surface, it would be the first to nucleate. However, the proposed heat pipe cannot possess such a large cavity. The tube wall itself will have cavities in the range of 10^{-3} to 10^{-4} inches as previously stated, and the largest cavity associated with the 150 mesh screen is the pore size itself; i.e., .002 inches.

---

* This number is based on conduction through methanol without giving effect to any contribution to conductance by the sintered wick.

If 0.002 inches is substituted into Equation (3-9), the critical ΔT becomes 1.75°F which still suggests a lack of ebullition.

4.0 MATERIALS

In selecting the materials for the heat pipe, the principal criteria were weight, fabricability, availability, thermal conductivity (in that it effects control) and, most important, compatibility.

Since methanol was to be the working fluid, materials compatibility-particularly in terms of gas evolution-- was of prime importance. At the design temperature range (65 $\pm$ 5°F) the heat pipe operates at relatively low pressure (1.44 - 1.96 psia), and very little gas generation would raise the operating temperature significantly.

In view of the above criteria, the following principal materials were selected for the AHPE.

Heat Pipe and Wicks:

Stainless steel was used for the pipe and wicks. It has a low thermal conductivity, which allowed developing the vapor-gas front over a short length of condenser; it is strong and available in thin-walled tubing (0.016 in.) for light weight; it is easily welded and sintered; and it is compatible with methanol, as demonstrated by life tests of sub-scale heat pipes [3].

Working Fluid:

Spectrophotometric grade methanol, selected for minimum water content, was used as the working fluid. Great care was taken in the process and fill operations to avoid contaminating the system with water, which could react with the stainless steel to liberate hydrogen.

Control Gas:

Research grade nitrogen (99.999% purity), seeded with a similar grade helium as a leak detection aid, was used as the control gas. Nitrogen was used to closely match the molecular weight of methanol (28 vs. 32) so as to avoid stratification of the vapor and gas in 1-g testing

and to minimize thermal diffusion effects. Oxygen, which would yield a closer match, was deemed unsuitable because of its chemical reactivity.

Radiator and Saddles:

The radiator and saddles were fabricated with aluminum because of its high thermal conductivity and light weight. The radiating surface was Alzak-Type M1, to provide thermal radiation properties consistent with the rest of the OAO-C spacecraft (α/ε = 0.17/0.75). The evaporator saddle was soldered to the heat pipe and the radiator was attached to clips on the condenser tube with RTV epoxy to facilitate removal for mounting on the spacecraft. The condenser tube clips were aluminum and were also soldered to the pipe. Their purpose was to increase the RTV interface area and thus the system conductance.

5.0 MECHANICAL DESIGN

The mechanical design of the AHPE had to be performed consistent with a series of internal and external constraints and requirements as follows:

1. The AHPE is mounted on the back surface of the OBP sink (honeycomb platform). Consequently, the position of the evaporator saddle and fasteners had to be consistent with the location of the OBP equipment so as to avoid interference.

2. The AHPE is not structurally connected to the OAO skin. A hole is cut in the skin to provide direct heat radiation to space by the AHPE radiator. Consequently, the dynamic displacement of the radiator under vibrational loading was constrained to a maximum amplitude of 0.5 inches to avoid interference with the solar arrays during launch.

3. The available volumetric envelope (28 X 16 X 3 1/2 in.) required that the condenser tube be bent 180 degrees on a small radius. The final design called for a 1.29 in. inside radius. The need to bend this tube without internal mandrels (after wick installation) established a minimum wall thickness to avoid buckling.

4. The evaporator, condenser and reservoir feed tubes had to withstand the maximum feasible internal pressure. This corresponded to a full power start-up at maximum boundary conditions with liquid in the reservoir. As shown on Figure 6, an upper bound for the pressure under these conditions is 22 psia.

5. The design goal for the total weight of the AHPE including attachments and radiator was 6.0 pounds, exclusive of fasteners and GSFC OAO modifications to the OBP and G1-Bay.

6. The AHPE had to withstand the vibration, shock, acceleration, and temperature environments specified in Table IV.

7. Additional constraints were imposed on materials selection and construction, workmanship, maintainability, etc., as specified in the

"Ames Variable Conductance Heat Pipe Performance and Interface Control Document", dated November 28, 1969.

The ultimate system design is shown on Drawing No. SK 122408, included with this report. No overall dynamic analysis was performed. Rather, structural and dynamic analyses were performed on potentially critical components. These analyses, included as Appendix C of this report, indicated that the design would meet all specifications.

Internal to the heat pipe, the principle methods of support were weldments and sintering of the wicks to the pipe walls.

External to the pipe, the radiator was supported by fiberglass structures tied directly to the aluminum evaporator saddle. The condenser tube did not contribute to the support of the radiator.

The radiator itself was fabricated of multiple individual fins. The fins of the primary radiator were channel shaped and epoxied together with fiberglass spacers for low axial conductivity. In addition, they were supported by fiberglass longerons running the length of the radiator. The smaller fins of the cold trap region were flat and not epoxied together to provide the lowest possible axial conductivity. In addition to the main longerons, these were supported by two additional outrigger longerons tying them to the primary radiator fins.

In addition to analytical pressure vessel calculations on the heat pipe tubing, a pressure proof test was performed on a simulated evaporator section of the AHPE. Analysis indicated that the weakest point in the system was the weld between the evaporator tube and the end cap containing the fill tube. Thus, a test element was fabricated and tested which simulated that region of the AHPE hardware. The results of hydrostatic testing showed a maximum tolerable pressure of about 400 psig. This is approximately twenty times the maximum anticipated pressure, indicating a large factor of safety. The pressure proof test procedure is presented in Appendix D.

Table IV

QUALIFICATION AND ACCEPTANCE TEST SPECIFICATIONS

VIBRATION

Qualification (All Axes)

Sinusoidal, 2 Octaves/Min.		Random, 4 Min./Axis	
FREQUENCY	LEVEL	FREQUENCY	LEVEL
5-24 Hz ±2% 24-100 Hz ±2% 110-2000 Hz ±2%	1/2" DA ±10% 15 g Peak ±10% 7.5 g Peak ±10%	15 Hz ±2% 15-70 Hz ±2% 70-100 Hz ±2% 100-400 Hz ±2% 400-2000 Hz ±2%	0.023 g^2/Hz ±10% Linear Increase 0.7 g^2/Hz ±10% Linear Decrease 0.045 g^2/Hz ±10%

Acceptance (All Axes)

Sinusoidal, 4 Octaves/Min.		Random, 4 Min./Axis	
FREQUENCY	LEVEL	FREQUENCY	LEVEL
5-20Hz ±2% 20-110 Hz ±2% 110-2000 Hz ±2%	1/2"DA ±10% 10.0g Peak ±10% 5.0 g Peak ±10%	15 Hz ±2% 15-70 Hz ±2% 70-100 Hz ±2% 100-400 Hz ±2% 400-2000 Hz ±2%	0.010 g^2/Hz ±10% Linear Increase 0.31 g^2/Hz ±10% Linear Decrease 0.02 g^2/Hz ±10%

NOTE: ONE SWEEP FOR EACH FREQUENCY.

SHOCK

Qualification

DIRECTION	LOAD	NO. SHOCKS	WAVE SHAPE	DURATION
Long. $+X_c$	30g ±10%	2	1/2 Sine	1 shock each axis 6ms 1 shock each axis 12ms
$-X_c$	30g ±10%	2		
Lat. $+Y_c$	15g ±10%	2		
$-Y_c$	15g ±10%	2		
$+Z_c$	15g ±10%	2		
$-Z_c$	15g ±10%	2		

ACCELERATION LEVELS

Qualification

DIRECTION	LOAD	DURATION
+X Axis	11.5g ±10%	4.5 Min/Axis
-X,±Y,±Z Axes	3.8g ±10%	

TEMPERATURE LEVELS

Qualification and Acceptance *

TEMPERATURE	CYCLES
-35°F ±5°F 140°F ±5°F	12

*Total duration of test shall be at least 48 hours.

6.0 DESIGN SUMMARY

The AHPE design is shown pictorially in Figures 11 and 12. Thermal energy from the OBP equipment platform is conducted through the aluminum saddle into the stainless steel heat pipe, where the methanol working fluid is vaporized. Energy released in condensing the vapor is rejected to space from the active portion of the condenser by the Alzak radiator. The condensed methanol is pumped back to the evaporator through a hybrid wicking system consisting of a "filled" artery in the condenser and multi-layer screen in the evaporator. Nitrogen, containing a small quantity of helium for leak detection, is the non-condensible control gas and is stored in the unwicked reservoir which is located inside the evaporator.

The effective axial conductivity of the condenser/radiator is reduced by splitting the radiator into channel segments and machining the condenser tube wall down to 0.016 in. in the gaps between them. The cold trap region uses a finer segment configuration to locally reduce the axial thermal conductance even further. The back of the primary radiator is painted black to provide a parallel heat transfer path to the radiator in the event of a heat pipe failure. However, the back of the cold trap region is insulated with aluminized mylar to lower its effective sink temperature and reduce the partial pressure of methanol in the gas reservoir.

The entrance to the reservoir is covered with a perforated Teflon plug to impede liquid from entering. However, should this occur the pipe can withstand the resulting pressure transient until the liquid automatically diffuses out. The reservoir feed tube is short and of large diameter to maximize the system transient response when diffusion is involved.

The AHPE was designed as an integral unit structurally, which interfaces with the OBP platform along the evaporator saddle only.

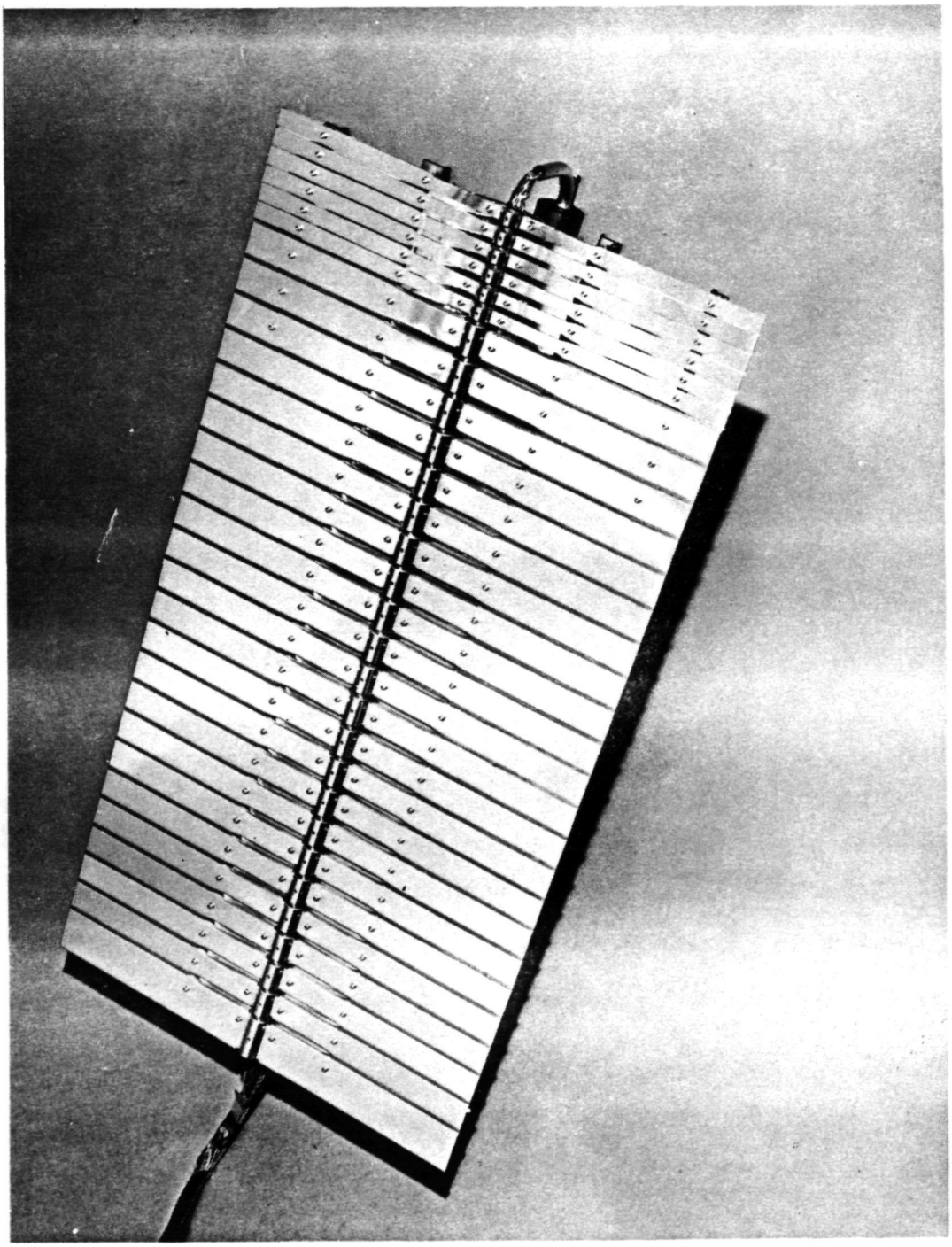

Figure 11. Photograph of AHPE

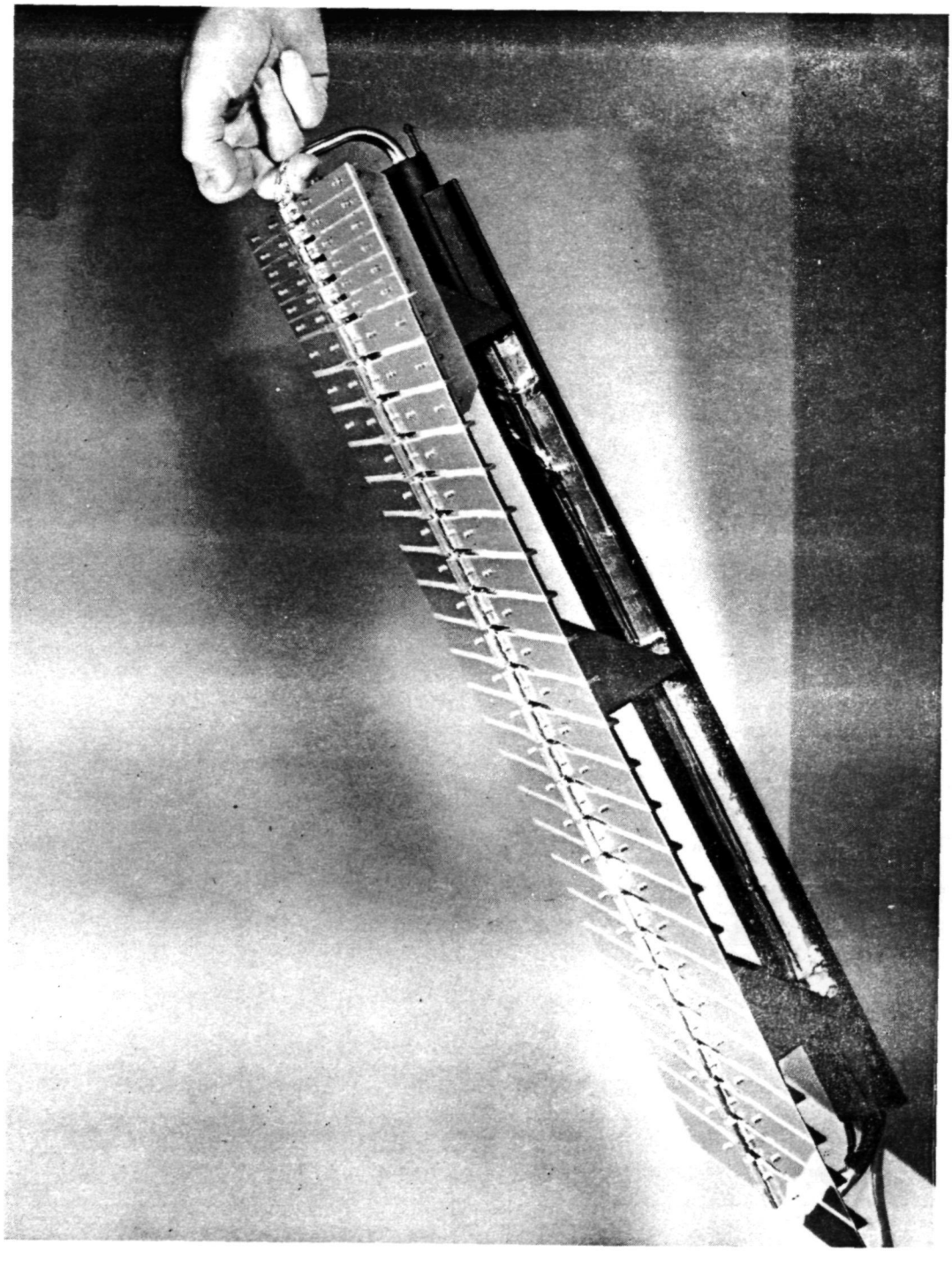

Figure 12. Photograph of AHPE

7.0 INSTRUMENTATION

For purposes of qualification and acceptance testing the AHPE heat pipes were instrumented with 23 copper-constantan thermocouples at various positions on the saddle, evaporator tube, reservoir feed tube and condenser. Heat input was supplied with either an electric heater plate mounted to the bottom of the saddle or electric strip heaters mounted to its sides.

Flight instrumentation consists of four thermistors, two on the evaporator and two on the condenser, as shown on Drawing No. SK 122408. Two strip heaters are mounted to the sides of the saddle, one with a 20 watt output and one with a 10 watt output at 28 volts. These heaters allow experimenting with the heat pipe independent of heat input from the OBP.

8.0 QUALIFICATION AND FLIGHT ACCEPTANCE TESTING

Tests were conducted on the qualification and flight units of AHPE according to the sequence shown in Table V.

TABLE V

TEST SEQUENCES

QUALIFICATION	ACCEPTANCE
Initial Leak	Initial Leak
Initial Functional	Initial Functional
Vibration	Vibration
Post Vibration Functional	Post Vibration Functional
Post Vibration Leak	Post Vibration Leak
Temperature Cycling	Temperature Cycling
Thermocouple Calibration	Thermocouple Calibration
Post Thermal Cycle Leak	Final Functional
Shock	Thermal Performance
Acceleration	
Final Leak	
Final Functional	
Thermal Performance	

A synopsis of test results was documented in [Reference 1]. Functional, leak, and thermal performance test procedures were the responsibility of TRW Systems and were defined in the following documents:

- AHPE Functional Test Procedure, No. AHPE-70-A-II, 28 May 1970
- AHPE Leak Test, No. AHPE-70-A-I, 28 May 1970
- AHPE Thermal Performance Test Procedure, No. AHPE-70-A-III, 1 June 1970

Procedures for the other tests listed in Table V were prepared by NASA-ARC.

9.0 REFERENCES

1. J. P. Kirkpatrick and B. D. Marcus, "A Variable Conductance Heat Pipe Flight Experiment", AIAA Paper No. 71-411, April 1971.

2. B. D. Marcus and G. Fleischman, "Steady State and Transient Performance of Hot Reservoir Gas-Controlled Heat Pipes", ASME Paper No. 70-HT/SpT-11, March 1970.

3. B. D. Marcus, "Theory and Design of Variable Conductance Heat Pipes: Hydrodynamics and Heat Transfer", Research Report No. 1, NASA Contract No. NAS 2-5503, April 1971.

4. B. D. Marcus, "Theory and Design of Variable Conductance Heat Pipes: Control Techniques", Research Report No. 2, NASA Contract No. NAS 2-5503, July 1971.

5. D. K. Edwards, G. L. Fleischman and B. D. Marcus, "User's Manual for the TRW Gaspipe Program", NASA CR-114306, April 1971.

6. D. K. Edwards and B. D. Marcus, "Heat and Mass Transfer in the Vicinity of the Vapor-Gas Front in a Gas-Loaded Heat Pipe", ASME Paper No. 71-WA/Ht-29, November 1971.

7. A. A. Westenberg, "A Critical Survey of the Major Methods for Measuring and Calculating Dilute Gas Transport Properties", Advances in Heat Transfer, Vol. III, Academic Press.

8. Hirschfelder, Curtiss and Bird, Molecular Theory of Gases and Liquids, Wiley, 1954.

10.0 NOMENCLATURE

A	-	Flow area
C	-	Pipe conductance
$\mathcal{D}_{vg}$	-	Mass diffusivity for vapor-gas pair
F	-	Crimping factor for screen mesh
J	-	Mechanical equivalent of heat
L	-	Length
M	-	Mesh size for screen (wires per inch), Molecular weight
P	-	Pressure
R	-	Thermal resistance
R_u	-	Universal gas constant
S	-	Safety factor
T	-	Temperature
T^*	-	Reduced temperature
V	-	Volume
$V_{\ell g}$	-	Difference in specific volumes of vapor and liquid
ΔP_c	-	Maximum capillary head
ΔP_c^*	-	Maximum value of capillary head along evaporator
ΔP_g	-	Gravity head
ΔP_o	-	Wick loading
ΔP_ℓ	-	Liquid pressure loss
ΔP_v	-	Vapor pressure loss
ΔT_{crit}	-	Critical superheat for nucleation

h	-	Coefficient of heat transfer
k	-	Thermal conductivity; Boltzmann's constant
m	-	Mass of vapor
$\dot{m}$	-	Mass flow rate
n	-	Number of moles of gas
q	-	Heat transfer rate
q/A	-	Radial heat flux into evaporator
r_n	-	Radius of critical nucleation cavity
t	-	Thickness
z	-	Axial Coordinate
α	-	Absorptivity
δ_{opt}	-	Optimum screen wire spacing
ε	-	Emissivity; Lennard-Jones potential parameter
ϕ	-	Porosity of wick
λ	-	Latent heat of vaporization
v_v	-	Velocity of vapor
$\Omega_{vg}^{(1,1)*}$	-	Collision integral for Lennard-Jones potential
ρ	-	Density
σ	-	Surface temperature; Lennard-Jones potential parameter
τ_D	-	Diffusion time constant

Subscripts (except when defined otherwise above):

c	-	Condenser
eff	-	Effective

ev	-	Evaporator
F	-	Reservoir feed tube
g	-	Gas
ℓ	-	Liquid
R	-	Reservoir
s	-	Effective sink
s'	-	Reservoir entrance
sat	-	Saturation
sct	-	Effective sink for cold trap
t	-	Tube wall
v	-	Vapor
w_c, w_e	-	Condenser and evaporator wall

APPENDIX A
DIFFUSION TIME CONSTANT: HEAT PIPE TRANSIENTS

It has been experimentally demonstrated that when working fluid vapor is present in significant quantities within the reservoir of hot reservoir, gas-controlled heat pipes, their transient response is dominated by diffusion of this vapor through the non-condensible control gas. The following analysis serves to generate an order-of-magnitude expression for the diffusion time constant which characterizes this process.

Assumptions:

(1) Geometry as shown in Figure A-1
(2) Quasi-steady state diffusion process
(3) Vapor pressure at entrance to feed tube is negligibly small compared with the partial pressure of vapor in the reservoir
(4) One-dimensional process
(5) Constant temperature and pressure

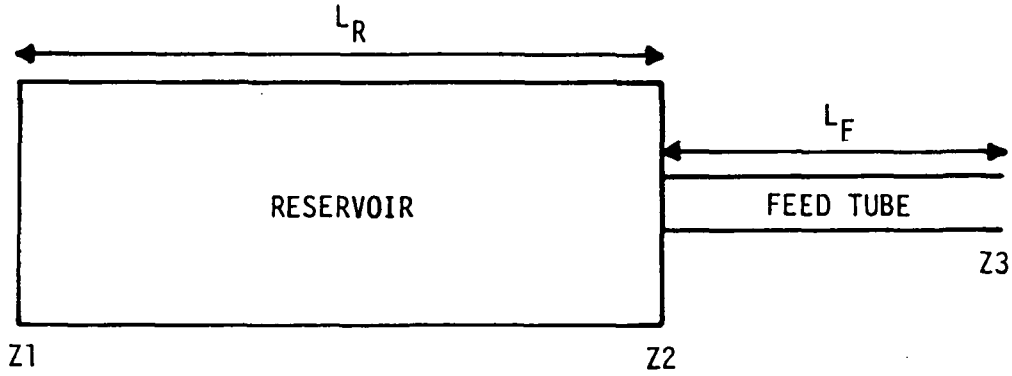

Figure A-1. Diffusion Model

The assumption of one-dimensional diffusion at constant pressure and temperature implies that Fick's first law applies in the following form:

$$\rho_v \mathcal{V}_v = - \mathcal{D}_{vg} \frac{d\rho_v}{dz} \qquad \text{(A-1)}$$

where:

ρ_v - density of vapor

$\mathcal{V}_v$ - velocity of vapor

z - axial coordinate

$\mathcal{D}_{vg}$ - mass diffusivity for vapor-gas pair

For a quasi-steady state process, the density gradients in both the reservoir and fill tube are linear. Thus, the axial fluxes of vapor in the reservoir and feed tube are given by:

$$\text{Reservoir:} \quad (\rho_v \mathcal{V}_v)_R = - \mathcal{D}_{vg} \left(\frac{\rho_{v_1} - \rho_{v_2}}{Z_2 - Z_1} \right) \qquad \text{(A-2a)}$$

$$\text{Feed tube:} \quad (\rho_v \mathcal{V}_v)_F = - \mathcal{D}_{vg} \left(\frac{\rho_{v_2}}{Z_3 - Z_2} \right) \qquad \text{(A-2b)}$$

where subscripts 1, 2 and 3 refer to the axial coordinates shown on Figure A-1. Note that ρ_{v_3} has been set equal to zero according to assumption 3.

At the interface between the reservoir and feed tube, conservation of mass requires that the mass flow rates be equal on each side. Thus,

$$(\rho_v \mathcal{V}_v)_R \; A_R = (\rho_v \mathcal{V}_v)_F \; A_F \qquad \text{(A-3)}$$

where:

A_R = flow area of reservoir

A_F = flow area of feed tube

If one now transposes Equations (A-2a) and (A-2b) to solve for $(\rho_{v_1} - \rho_{v_2})$ and ρ_{v_2} respectively, and then sums the two results, Equation (A-4) is obtained:

$$\rho_{v_1} = \frac{-(Z_2 - Z_1)\ (\rho_v \mathcal{V}_v)_R \ -(Z_3 - Z_2)\ (\rho_v \mathcal{V}_v)_F}{\mathcal{D}_{vg}} \qquad \text{(A-4)}$$

Now, substituting Equation (A-3) for $(\rho_v \mathcal{V}_v)_R$ into Equation (A-4), and noting that $(Z_2 - Z_1) = L_R$ and $(Z_3 - Z_2) = L_F$, one obtains:

$$\rho_{v_1} = \frac{\left(-L_R \frac{A_F}{A_R} - L_F\right)\ (\rho_v \mathcal{V}_v)_F}{\mathcal{D}_{vg}} \qquad \text{(A-5)}$$

Finally, solving Equation (A-5) for $(\rho_v \mathcal{V}_v)_F$ and multiplying by A_F yields the mass rate of vapor flow out of the system:

$$\dot{m} = A_F\ (\rho_v \mathcal{V}_v)_F = \frac{-\mathcal{D}_{vg}\ A_F\ \rho_{v_1}}{L_F + \frac{A_F}{A_R}\ L_R} \qquad \text{(A-6)}$$

It is now necessary to obtain an expression for the mass of vapor in the system in terms of ρ_{v_1} so that the mass flow rate can be expressed in terms of the vapor inventory itself: The assumption of linear gradients (quasi-steady state) yields:

$$m = \frac{(\rho_{v_1} + \rho_{v_2})}{2} V_R + \frac{\rho_{v_2} V_F}{2} \qquad \text{(A-7)}$$

$$= \frac{\rho_{v_1} V_R}{2} + \frac{\rho_{v_2}}{2} (V_R + V_F)$$

where V_R and V_F are the volumes of the reservoir and fill tube respectively.

Performing a little algebra with Equations (A-2) and (A-5) yields an expression for ρ_{v_2}:

$$\rho_{v_2} = \frac{L_F \rho_{v_1}}{\left(L_R \frac{A_F}{A_R} + L_F\right)} \qquad \text{(A-8)}$$

Now, substituting Equation (A-8) into Equation (A-7) yields:

$$m = \frac{\rho_{v_1} V_R}{2} \frac{L_F \rho_{v_1}}{\left(L_R \frac{A_F}{A_R} + L_F\right)} \left(\frac{V_R + V_F}{2}\right) \qquad \text{(A-9)}$$

Solving Equation (A-9) for ρ_{v_1}, substituting into Equation (A-6), and performing some additional algebra yields:

$$\dot{m} = \frac{-\mathcal{D}_{vg}\, m}{\frac{V_R L_F}{A_F} + \frac{(L_F^2 + L_R^2)}{2}} \qquad \text{(A-10)}$$

This expression is simply a first order, linear differential equation yielding an exponential solution with time constant:

$${}^{\tau}\mathcal{D} = \left[\frac{V_R L_F}{A_F} + \frac{(L_R^2 + L_F^2)}{2} \right] \frac{1}{\mathcal{D}_{vg}} \qquad \text{(A-11)}$$

This is the required expression for the diffusion time constant of the heat pipe.

APPENDIX B

MASS DIFFUSION

Available references do not provide any experimental data on binary diffusion between methanol and nitrogen. Consequently, it was necessary to calculate the mass diffusivity from first principles.

From kinetic theory, using the Lennard-Jones (12-6) potential energy function, the basic binary diffusion coefficient for non-polar: non-polar and polar: non-polar gas pairs is given by [7].

$$\mathcal{D}_{vg} = \frac{1.86 \times 10^{-3} \left[(M_v + M_g)/M_v M_g\right]^{1/2} T^{3/2}}{P \, \sigma_{vg}^2 \, \Omega_{vg}^{(1,1)*}} \qquad \text{(B-1)}$$

where:

$\mathcal{D}_{vg}$ - Mass diffusivity for the v-g gas pair - (cm^2/sec)

M_v, M_g - Molecular weights

T - Absolute temperature (°K)

P - Absolute pressure (atmospheres)

σ_{vg}^2 - Lennard-Jones potential parameter

$\Omega_{vg}^{(1,1)*}$ - Collision integral for Lennard-Jones potential

The parameter $\Omega_{vg}^{(1,1)*}$ is tabulated in the literature [8] as a function of the reduced temperature:

$$T^* = \frac{T}{(\epsilon/k)_{vg}} \qquad \text{(B-2)}$$

where:

ε - Lennard-Jones potential parameter

k - Boltzmann's constant

The two Lennard-Jones parameters, σ_{vg} and ε_{vg} are also unavailable for the methanol-nitrogen gas pair. However, the individual parameters σ_{vv}, σ_{gg}, ε_{vv} and ε_{gg} are available from measured viscosity data [7]. Using the individual parameters, and the following combining rules, one can obtain the necessary values to calculate $\mathscr{D}_{vg}$ from Equation (B-1).

$$\varepsilon_{vg} = (\varepsilon_{vv}\ \varepsilon_{gg})^{1/2}$$

$$\sigma_{vg} = 1/2\ (\sigma_{vv} + \sigma_{gg}) \qquad \text{(B-3)}$$

Table B-1 presents the results of this calculation for the pressure-temperature combination of importance in the AHPE heat pipe design.

The pressure selected is the total pressure in the heat pipe at an operating temperature of 70°F, the high end of the nominal control range. However, since the actual diffusion process occurs across a temperature gradient from 70°F at the reservoir to -19°F at the end of the cold trap, the latter value was used to calculate $\mathscr{D}_{vg}$. As seen in Equation (B-1), this yields a conservative (low) value for $\mathscr{D}_{vg}$.

The temperature difference across the reservoir feed tube can also lead to a thermal diffusion phenomenon wherein a mixture of gases at constant pressure tends to separate due to a temperature gradient [4]. However, calculations indicated that this effect would be insignificant in the AHPE system.

TABLE B-1

MASS DIFFUSIVITY CALCULATIONS

P (psia)	T (°F)	P (atmos)	T (°K)	T*	$\Omega_{vg}^{(1,1)}$	$\mathscr{D}_{vg}$ (cm^2/sec)	$\mathscr{D}_{vg}$ (ft^2/hr)
1.95	-19	.1325	244	1.32	1.32	.789	3.06

v - methanol (CH_3OH) $M_v = 32$

g - nitrogen (N_2) $M_g = 28$

$\sigma_{vv} = 3.63\text{Å}$ $\sigma_{gg} = 3.80\text{Å}$ $\sigma_{vg} = 3.72\text{Å}$

$(\varepsilon/k)_{vv} = 482°K$ $(\varepsilon/k)_{gg} = 71°K$ $(\varepsilon/k)_{vg} = 185°K$

APPENDIX C

DESIGN STRUCTURAL/DYNAMIC ANALYSIS

The following analysis was performed to assure that the OAO Heat Pipe Experiment (AHPE) satisfies structural requirements. The analysis is based on the following information:

- o Design: Drawing SK 122408, dated 25 March 1970.
- o Environment: AMES Interface spec, dated 28 November 1969.
- o Critical Condition: 7.5 g sine vibration input 70-100 Hz.
- o Design Weight: 6.0 lb. total, 2.0 lb structurally supported.

The design criteria for structural and dynamic analysis is an equivalent quasi-static loading of 75 g's in any axis (Q = 10 transmissibility) and a first mode frequency above 150 Hz. All analysis was performed on potentially critical components with no overall dynamic model being used. Three potentially critical modal responses were investigated (modal coupling was assumed small).

1. First-mode beam response of panel fins.
2. Simple supported beam response of supported tube.
3. Axial response of panel assembly on supports.

Results of the analysis indicates 276 Hz first mode frequency and a minimum margin of safety of +.23 (local bending at the fin attachments).

TRW SYSTEMS GROUP
ONE SPACE PARK • REDONDO BEACH, CALIFORNIA

PREPARED D.G. CROSS 4/2/70 REPORT NO. PAGE 1

CHECKED

MODEL OAO HEAT PIPE EXP

CONFIGURATION

DESIGN

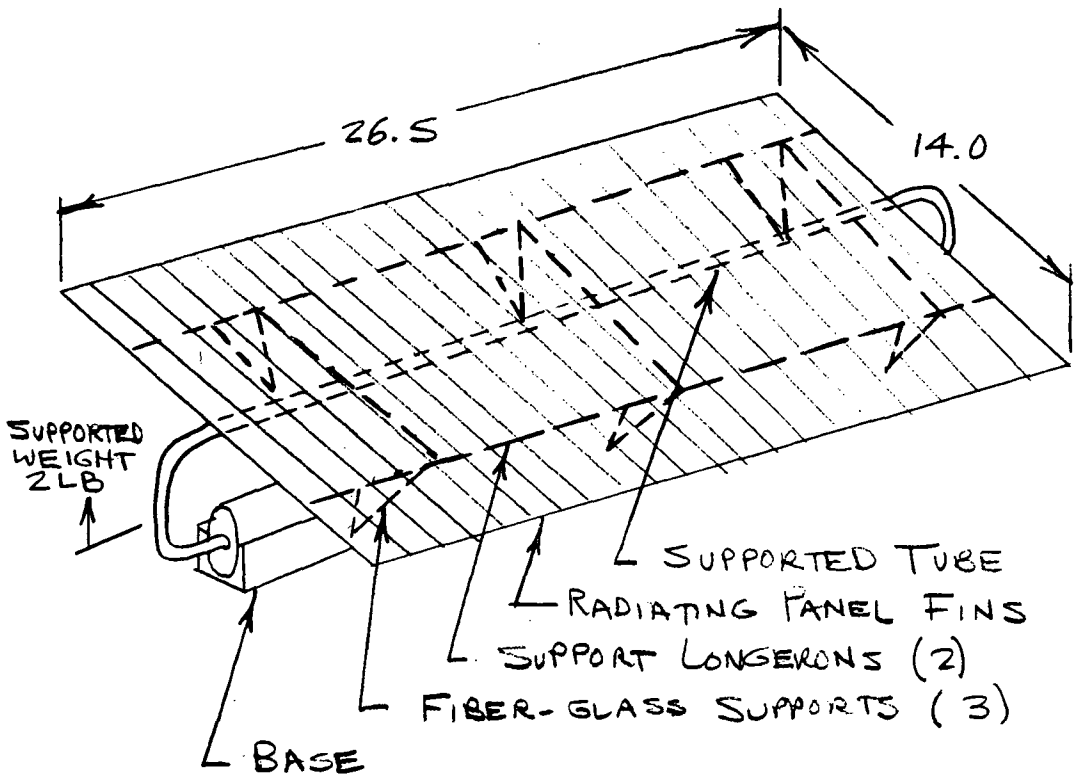

SYSTEMS 1441 REV. 8-67

TRW SYSTEMS GROUP
ONE SPACE PARK · REDONDO BEACH, CALIFORNIA

PREPARED D. G. CROSS 2/26/70 REPORT NO. PAGE 2

CHECKED

MODEL OAO HEAT PIPE EXP.

DESIGN LOADS

Flight Loads

Shock

30 g's long. half-sine with $\tau = .006$ sec ①
OR .012 sec ②

Assume $f_n = 150$ cps
OR $\tau_n = .0067$ sec

$\beta \equiv 2\tau/\tau_n = 1.79$ ①
OR 3.58 ②

Shock Response Factor = 1.76, $\gamma = 53$ g's ①
OR 1.35, $\gamma = 41$ g's ②
Assuming no structural damping

Sine Vibration, Peak Qual.

15 g's 24-110 Hz
7.5 g's ≥110 Hz

Vibration Response @ $f_n > 110$ Hz, $Q = 10$
$\gamma = 75$ g's

RESULTING DESIGN CRITERIA
- STRUCTURAL LOADS & STIFFNESS

1. Loading : $\gamma = 75$ g's ult.
2. Stiffness : $f_n > 150$ Hz first natural freq.

SYSTEMS 1441 REV. 8-67

TRW SYSTEMS GROUP
ONE SPACE PARK • REDONDO BEACH, CALIFORNIA

PREPARED D. G. CROSS 3/27/70 REPORT NO. PAGE 3

CHECKED

MODEL OAO HEAT PIPE EXP.

STRUCTURAL / DYNAMIC ANALYSIS

RADIATING PANEL- FINS MODEL RESPONSE

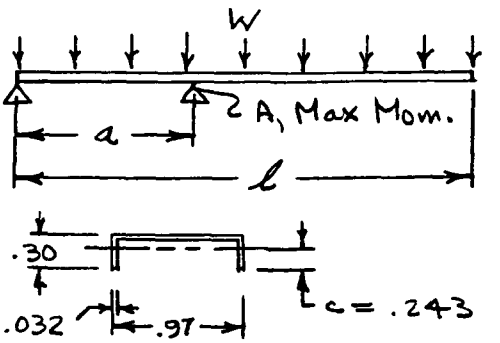

$W = .040$ lb, each fin
$\ell = 7.0$ in
$a = 2.5$ in
$\gamma = 75$ g
$E = 10 \times 10^6$ psi
$f_n > 150$ Hz, goal

CROSS-SECTION : $I = .412 \times 10^{-3}$ in^4

NATURAL FREQUENCY

$$f_n = C\sqrt{\frac{EI}{W\ell^3}} \quad ; \quad C = f(a/\ell) = 20.6 \text{ @ } a/\ell = .36$$

$$f_n = 20.6\left[\frac{(10\times10^6)(.412\times10^{-3})}{(4.0\times10^{-2})(.7\times10^{1})^3}\right]^{1/2} = \underline{356 \text{ Hz}}, \text{ WITH PIN SUPPORTS!}$$

BENDING STRESS @ A

$$M = \frac{W\gamma}{2\ell}(\ell - a)^2 = \frac{(.040)(75)(4.5)^2}{2(7.0)} = 4.34 \text{ in-lb}$$

$$f_b = \frac{Mc}{I} = \frac{4.34\,(.243)}{4.12\times10^{-3}} = \underline{256 \text{ psi}}$$

Non-Critical

SYSTEMS 1441 REV. 8-67

TRW SYSTEMS GROUP
ONE SPACE PARK • REDONDO BEACH, CALIFORNIA

PREPARED D. G. CROSS 3/20/70 REPORT NO. PAGE 4

CHECKED

MODEL OAO HEAT PIPE EXP.

STRUCTURAL / DYNAMIC ANALYSIS

SUPPORTED TUBE

Model

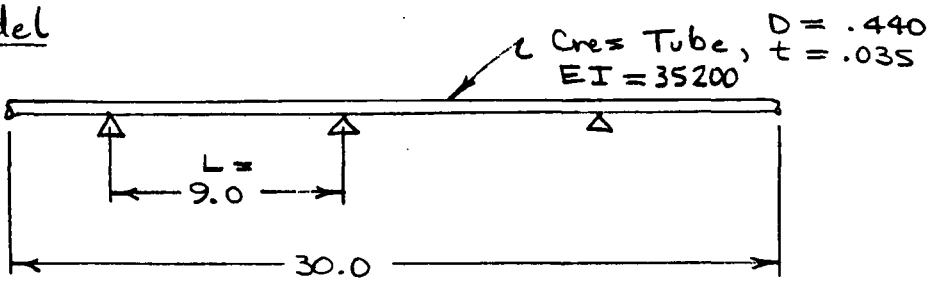

W = 2.0 lb

w = .067 lb/in

Natural Frequency, Distributed-Weight Beam

$$f_n = C\sqrt{\frac{EI}{wL^4}} \quad ; \quad C = 30.8 \text{ pin-ended} \quad = 68.7 \text{ clamped-end}$$

$$f_n = 30.8\left[\frac{.352\times10^5}{(.67\times10^{-1})(.9\times10^1)^4}\right]^{1/2} = \underline{276 \text{ Hz}} \text{ min.}$$

Maximum Bending Stress @ γ = 75 g's ult.

$f = M/Z \quad ; \quad Z = \frac{\pi}{4}D^2t = .0532 \text{ in}^3$

$M = \frac{1}{8}\gamma w L^2 = .125(75)(.067)(9)^2 = 50.9 \text{ in-lb}$

$f = 50.9/.0532 = \underline{960 \text{ psi}}$ Non-Critical

TRW SYSTEMS GROUP
ONE SPACE PARK • REDONDO BEACH, CALIFORNIA

PREPARED D. G. CROSS 3/27/70 REPORT NO. PAGE 5

CHECKED

MODEL OAO HEAT PIPE EXP.

STRUCTURAL / DYNAMIC ANALYSIS

SIDE - SUPPORT LONGERON

CASE 1

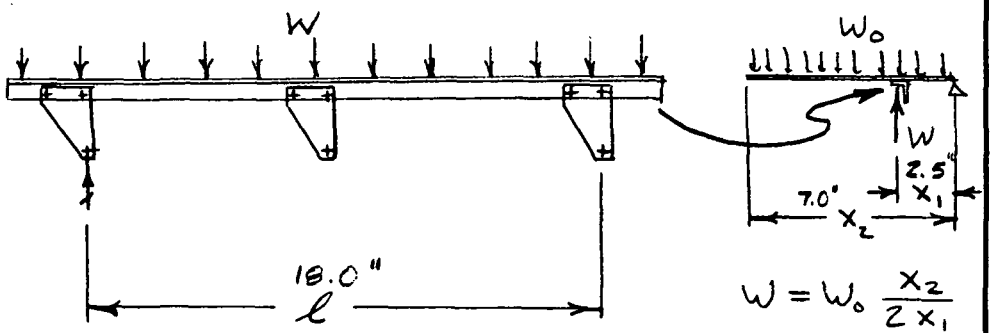

$$W = W_o \frac{X_2}{2X_1}$$

$W_o = (1.0\ \text{lb fin weight})(\tfrac{1}{2})(75\ g's) = 37.5\ \text{lb}$

$W = 37.5\ (7.0) / (2(2.5)) = 52.5\ \text{lb}$

$M = \frac{1}{32} W\ell = (\frac{1}{32})(52.5)(18.0) = 29.6\ \text{in-lb}$

$c = .527\ \text{in}, \quad I = .0619\ \text{in}^4$

$f_b = 29.6\left(\frac{.527}{.0619}\right) = \underline{252\ \text{psi}}$ Non-Critical

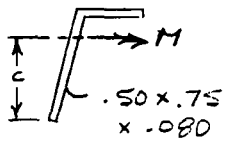

CASE 2

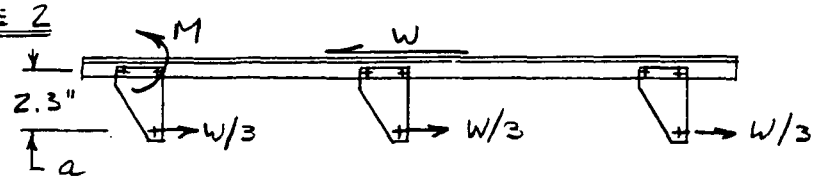

$W = (2.0\ \text{lb supported weight})(\tfrac{1}{2})(75\ g's) = 75\ \text{lb}$

$M = \frac{1}{3}(75\ \text{lb})(2.3\ \text{in}) = 57.6\ \text{in-lb}$

$f_b = 57.6\left(\frac{.527}{.0619}\right) = \underline{490\ \text{psi}}$ Non-Critical

$K = 18EI/a^2\ell = 18(10^7)(.0619)/(2.3)^2(18) = 1.17 \times 10^5\ \frac{\text{lb}}{\text{in}}$

$M = \frac{1}{2}(2\ \text{lb}) / 386 = .00259\ \text{lb-sec}^2/\text{in}$

$f_n = \frac{1}{2\pi}\sqrt{K/M} = 1070\ \text{Hz}$ NATURAL FREQUENCY ALONG PIPE

SYSTEMS 1441 REV. 8-67

TRW SYSTEMS GROUP
ONE SPACE PARK • REDONDO BEACH, CALIFORNIA

PREPARED D.G. CROSS 3/27/70 REPORT NO. PAGE 6

CHECKED

MODEL OAO HEAT PIPE EXP

STRUCTURAL / DYNAMIC ANALYSIS

FIBER-GLASS TUBE SUPPORTS

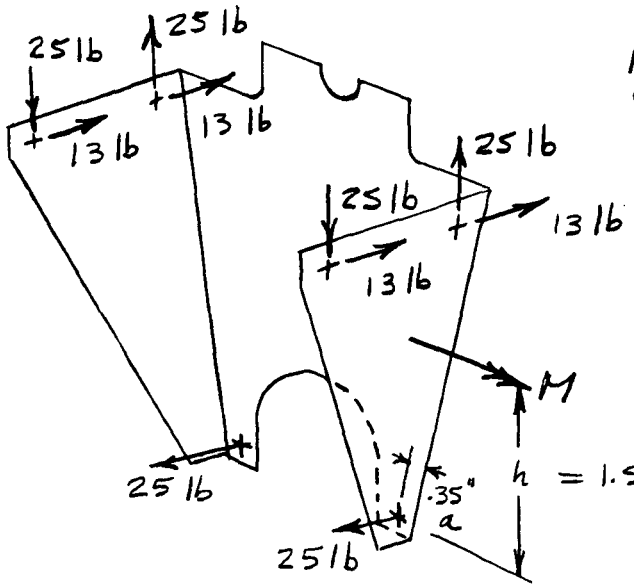

AXIAL LOAD CASE CRITICAL

Compressive Stress in Edge

$M = 2(25\ lb)(1.5\ in) = 75\ in\text{-}lb$

$I = .124\ in^4,\ c = 1.28\ in$

$f_b = 75\left(\frac{1.28}{.124}\right) = \underline{770\ psi}$

NON-CRIT.

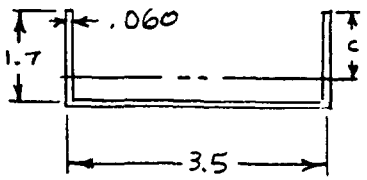

Bending Stress at Bolts

$b_{eff} = .50\ in$;

$Z = \frac{1}{6}bt^2 = \frac{1}{6}(.50)(.06)^2 = 3\times10^{-4}\ in^3$

$M = \frac{1}{2}Pa = \left(\frac{1}{2}\right)(25\ lb)(.35) = 4.4\ in\text{-}lb$

$f_b = 4.4/(3\times10^{-4}) = \underline{15000\ psi}$

$F_b = 45000\ psi$ NON-CRITICAL

SYSTEMS 1441 REV. 8-67

TRW SYSTEMS GROUP
ONE SPACE PARK • REDONDO BEACH, CALIFORNIA

PREPARED D. G. CROSS 3/30/70 REPORT NO. PAGE 7

CHECKED

MODEL CAO HEAT PIPE EXP.

STRUCTURAL / DYNAMIC ANALYSIS

CRITICAL LOCAL JOINTS

1. END CAP OF MAIN TUBE UNDER 20 psi PRESSURE

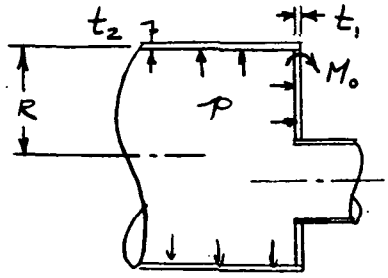

Roark Table XIII
Case 24, pg 274

$t_1 = .035$ in
$t_2 = .035$ in
$R = .219$ in.

$$f_b = 6M_o/t_2^2 + pR/2t_2$$

$$M_o = pR^2\left[\frac{A/B + BC}{\lambda + A - B/2}\right]$$

where $\lambda = \left(\frac{3(1-\nu^2)}{R^2 t_2^2}\right)^{1/4}$

$$D = \left(\frac{Et^3}{12(1-\nu^2)}\right)$$

$$A = \frac{R\lambda^2 D_2}{(1+\nu)D_1}$$

$$B = \frac{\lambda E t_1}{Et_1 + 2D_2\lambda^3 R(1-\nu)}$$

$$C = \frac{\lambda^2 D_2}{Et_2(1-\frac{1}{2}\nu)}$$

CALCULATIONS

A small on-line computer program was utilized using TYMESHARE'S Superbasic language to calculate corner bending stress —

```
 RUN
DISCONTINUITY STRESSES AT THE CORNER OF A FLAT
HEADED CYLINDRICAL PRESSURE VESSEL; ROARK TABLE XIII
CASE 24, PAGE 274, 3RD ED.

INPUT E, NU, P, R, T1, T2
? 30E6, .30, 20, .219, .035, .035
CYLINDER AXIAL+ BENDING STRESS AT CORNER   583.03966 PSI
                                          NON-CRITICAL
ARE NEW VALUES OF T1 AND T2 TO BE RUN? (1=YES; 0=NO)
? 1
INPUT T1, T2
? .050, .035
CYLINDER AXIAL+ BENDING STRESS AT CORNER   512.37305 PSI

ARE NEW VALUES OF T1 AND T2 TO BE RUN? (1=YES; 0=NO)
? 0
```

SYSTEMS 1441 REV. 8-67

TRW SYSTEMS GROUP
ONE SPACE PARK • REDONDO BEACH, CALIFORNIA

PREPARED D. G. CROSS 3/30/70 REPORT NO. PAGE 8

CHECKED

MODEL CAO HEAT PIPE EXP.

STRUCTURAL / DYNAMIC ANALYSIS

CRITICAL LOCAL JOINTS (CON'D)

2. ATTACH - LOOPS OF FINS TO TUBE

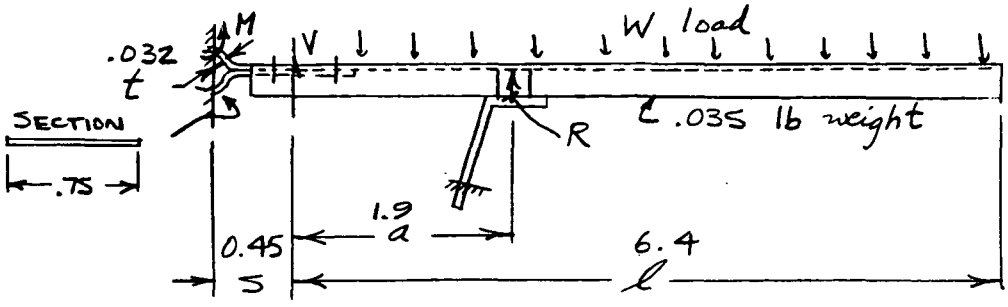

$W = 75\ g's\ (.035\ lb) = 2.6\ lb$

$V = W\left(\frac{\ell}{2a} - 1\right) = 2.6\left(\frac{6.4}{.90} - 1\right) = 15.9\ lb$

$M = \frac{1}{4} Vs = \frac{1}{4}(15.9)(0.45) = 1.8\ in\text{-}lb$

$Z = \frac{1}{6} bt^2 = \frac{1}{6}(.75)(.032)^2 = .000128\ in^3$

$f_b = \frac{1.8}{1.28 \times 10^{-4}} = \underline{14100\ psi}$ US

$F_{ty} = 20000\ psi$ for 3003 Aluminum H16 Condition

$M.S. = \underline{+.42}$

3. PLATE BENDING STRESS AT INTER. SUPPORT

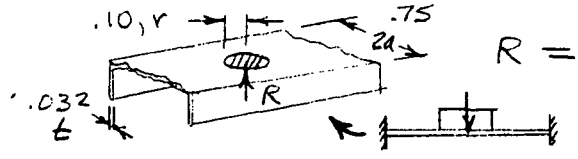

$R = W + V = 18.5\ lb$

Roark Table X, Case 20

$f_b = \beta R/t^2$; $\beta = .90$ @ $a/r = 3.75$

$= .90(18.5)/(.032)^2 = 16260\ psi$

$M.S. = \underline{+.23}$

APPENDIX D

PRESSURE PROOF TEST OF AHPE HARDWARE

A pressure proof test was performed on a simulated evaporator section of the Ames Heat Pipe Experiment to assure structural integrity under worst case conditions.

Analysis indicated that the weakest point on the AHPE system was the weld between the evaporator tube and the end cap containing the fill tube. Thus, a test element was fabricated and tested which simulated that region of the AHPE hardware.

Fabrication:

The materials and procedures used to fabricate the test element were identical to those of the AHPE hardware as described on Drawing No. SK 122408, Rev. B, in almost every respect. The only meaningful difference was that the test element did not have any wicking, which might provide the actual hardware with additional support.

A sketch of the test element is shown in Figure D-1. The fabrication procedure was as follows:

1. Machined all piece parts.
2. Cleaned all parts according to MSD: 70-A spec.
3. Vacuum fired all parts at 1253°C for 30 minutes.
4. Welded assembly (TIG weld).
5. Stress relieved at 570°F for 16 hours.
6. Pinched-off fill tube.

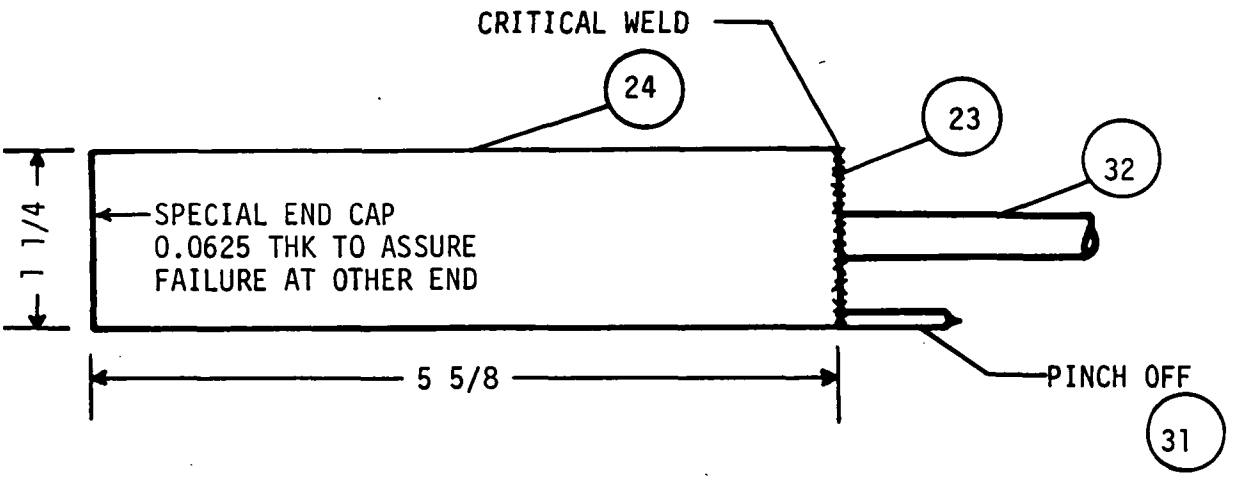

FIGURE D-1. Sketch of Test Element.

Test:

The test specimen was included in a hydraulic pressure test apparatus shown schematically in Figure D-2.

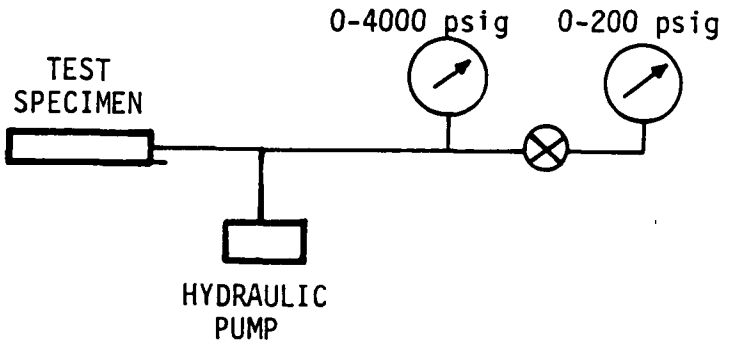

FIGURE D-2. Schematic of Test Set-Up.

The test procedure was simply to increase the pressure in the system and observe the results. The principal results can be summarized as follows:

1) No observable effect was recorded until the end cap bulged and the weld yielded at approximately 450 psig.

2) At 1300 psig the test specimen was thoroughly deformed, but with no weld or pinch off failures.

Conclusion:

The test showed a maximum tolerable pressure of about 400 psig. This is approximately twenty (20) times the maximum anticipated pressure for the AHPE, providing a large factor of safety.